In search of an ice-core signal to differentiate between source-driven and sink-driven changes in atmospheric methane

Levine, J. G.[1], E. W. Wolff[1], A. E. Jones[1], M. A. Hutterli[1,*], O. Wild[2], G. D. Carver[3, 4], and J. A. Pyle[3, 4]

[1]British Antarctic Survey, High Cross, Madingley Road, Cambridge, UK
[2]Lancaster Environment Centre, University of Lancaster, UK
[3]Centre for Atmospheric Science, Department of Chemistry, University of Cambridge, UK
[4]National Centre for Atmospheric Science, University of Cambridge, UK
[*] {Now at TOFWERK AG, Uttigenstrasse 22, CH-3600 Thun, Switzerland}
Correspondence to: J. G. Levine (javi@bas.ac.uk)

Abstract

The concentration of atmospheric methane increased from around 360 ppbv at the last glacial maximum (~20ka before present) to about 700 ppbv in the pre-industrial era (~200a before present). The sources and/or sinks of methane must therefore have changed during this period, however, the relative sizes of the source- and sink-driven changes in methane concentration remain uncertain. We take the first 'bottom-up' approach to identifying any chemical signals preserved in the ice record that could help us to determine these. Using an atmospheric chemistry-transport model, we explore the effects of source- and sink-driven changes in methane on a wide range of chemical species in the Antarctic boundary layer. Though we identify several potentially useful atmospheric signals, a simple and robust constraint on the sizes of the source- and sink-driven changes cannot be readily identified, owing to: their preservation in the ice; limitations to the information they hold;

and/or ambiguity surrounding their interpretation. This includes the mass-independent fractionation of oxygen isotopes in sulfates, and the concentration of formaldehyde, in which there has been considerable interest. Our exploration is confined to a domain in which NO_x emissions and climate remain constant. However, given the uncertainties associated with the changes in these factors, we would anticipate their inclusion to make it harder still to identify a robust signal. Finally, though formaldehyde cannot provide this, we propose how it might be used to synchronize the gas- and aqueous-phase Antarctic-ice records, and thus determine the relative phasing of glacial-interglacial changes in southern-hemisphere CO_2 and temperature.

1 Introduction

The concentration of atmospheric methane trapped in Antarctic ice shows large variations over the last 800,000 years that appear to track changes in temperature on orbital, and shorter, timescales [Jouzel et al., 2007; Loulergue et al., 2008]; see, for example, Chappellaz et al. [1993a], for details of the phase relationship between changes in methane and climate in Greenland. This study focuses on the increase in methane from around 360 ppbv at the last glacial maximum (LGM; ~20ka before present) to approximately 700 ppbv in the pre-industrial era (PI; ~200a before present). Fundamentally, the increase must have resulted from a change in methane sources, such as emissions from wetlands—the largest natural source of methane, and/or a change in methane sinks, the dominant one being oxidation by the hydroxyl radical (OH), but the balance between these changes remains uncertain. Our aim is to identify any atmospheric chemical signals that could be used to differentiate between changes in methane emissions and changes in OH, and assess the likelihood they are preserved in Antarctic ice.

Estimates of the changes in methane emissions between the LGM and the PI vary, with much of the discussion focusing on the change in emissions from wetlands. Based on a reconstruction of vegetation, Chappellaz et al. [1993b] estimated that wetland emissions increased by 80% between the LGM and the PI, underpinning a 46% increase in total methane emissions that could explain around half the 94% increase in methane concentration (from 360 to 700 ppbv). Bottom-up studies employing dynamic global vegetation models, on the other hand, have calculated much smaller increases in wetland emissions, ranging from effectively no change [Kaplan et al., 2006] to an increase of 36% [Valdes et al., 2005], and consequently more modest increases in total methane emissions, of 19% and 31% respectively. Recent calculations by Weber et al. [2010], based on climate simulations from the second phase of the Paleoclimate Modelling Intercomparison Project (PMIP2) [Braconnot et al., 2007], suggest wetland emissions increased by between 54 and 72%,

and highlight the uncertainty that remains in the size of the source-driven component of the LGM-PI change in methane concentration.

The estimated changes in methane emissions cited above suggest changes in methane sources alone cannot fully account for the LGM-PI change in methane, and a significant fraction of this must have been sink-driven (i.e. the result of an increase in the atmospheric lifetime of methane). Valdes et al. [2005] and Kaplan et al. [2006] showed how the concentration of OH could have decreased, and hence the lifetime of methane increased, as a result of an increase in the amount of non-methane volatile organic compounds (NMVOCs) emitted from vegetation. An increase in NMVOC emissions between the LGM and the PI is consistent with vegetation reconstructions [see, e.g., Adams et al., 2001] and model studies of the influence that rising temperatures have on vegetation [e.g. Lathière et al., 2005]. However, the size of this increase remains uncertain [see, e.g., Arneth et al., 2007], since some laboratory studies have identified a reduction in NMVOC emissions as the concentration of CO_2 to which vegetation is exposed is increased [e.g. Wilkinson et al., 2009], and the concentration of CO_2 rose between the LGM and the PI [Monnin et al., 2001]. The possible 'recycling' of OH consumed in isoprene oxidation [Lelieveld et al., 2008] adds to the uncertainty in the influence NMVOC emissions had on OH and, hence, the size of the sink-driven component of the change in methane concentration.

Changes in the amount of nitrogen oxides (NO_x=NO+NO_2) emitted from climate-sensitive sources, such as soils, lightning and biomass burning, could have also affected the lifetime of methane with respect to OH. All else being equal, we would expect an increase (decrease) in NO_x emissions to have led to an increase (decrease) in the concentration of ozone (O_3), and hence an increase (decrease) in the concentration of OH, since OH is formed from the reaction between excited $O(^1D)$ oxygen atoms (derived from O_3) and water vapor. Valdes et al. [2005] estimated that NO_x emissions from lightning increased from 3.4 to 4.2 Tg N $year^{-1}$, whilst those from soils decreased

88 from 5.7 to 5.1 Tg N $year^{-1}$, leading to an overall 6% reduction in the lifetime of methane in the PI,
89 relative to the LGM. However, their estimates of the lightning and soil source strengths are subject
90 to large uncertainties; the emissions from lightning, to which the lifetime of methane is especially
91 sensitive, are uncertain in the present, never mind the past [Wild, 2007]. It is also unclear how NO_x
92 emissions from biomass burning changed during this period. Calculations by Thonicke et al. [2005]
93 using a dynamic global vegetation model with an embedded fire module suggested these could have
94 decreased in the tropics, and thus contributed to an increase in the lifetime of methane. However,
95 based on a suite of Monte-Carlo calculations, Fischer et al. [2008] concluded that the amount of
96 biomass burning was roughly constant between the LGM and the PI, and a global synthesis of
97 charcoal records by Power et al. [2008] identified the last glacial period (16-21ka before present) as
98 the period of least biomass burning in the last 21kyr, and hence an increase in biomass-burning
99 emissions from the LGM to the PI.
100
101 The change in climate itself would have also affected the lifetime of methane. Contrary to the
102 increase that could help to explain the observed increase in methane concentration, the increase in
103 temperatures, and hence humidities, would have tended to reduce the lifetime of methane by
104 increasing the (temperature-dependent) rate of reaction between OH and methane, and increasing
105 the concentration of OH. Martinerie et al. [1995] estimated that the increase in humidity would
106 have led to a 6% reduction in the lifetime of methane, whilst Valdes et al. [2005] estimated that this,
107 together with the increased rate of reaction between OH and methane, would have led to a reduction
108 of 14%. These estimates, however, are subject to significant uncertainties in the changes in
109 temperature between the LGM and the PI [e.g. Braconnot et al., 2007], particularly in the tropics
110 where roughly three quarters of methane oxidation occurs [see, e.g., Lawrence et al., 2001;
111 Labrador et al., 2004]. Proxy data collated and analysed within the Multiproxy Approach for the
112 Reconstruction of the Glacial Ocean Surface Project [MARGO Project Members, 2009] show an
113 average sea-surface-temperature warming between 15°N and 15°S of 1.7(±1.0)°C between the

LGM and the PI, and the large, relative uncertainty in this figure (almost 60%) is echoed in the wide range of warmings exhibited by state-of-the-art climate models, from 1.0 to 2.4°C [Otto-Bliesner et al., 2009]. What is not in question, is that the warming climate would have tended to reduce the lifetime of methane. The most likely explanation identified in the literature for a net increase in methane lifetime from the LGM to the PI, which would help to explain the increase in methane concentration, depends upon an increase in NMVOC emissions (discussed above).

Previous observational studies suggesting the concentration of OH has changed in the past have largely taken a 'top-down' approach, attributing changes in the concentration, or isotopic composition, of atmospheric constituents trapped or dissolved in polar ice to changes in oxidizing capacity. A variety of chemical signals with which to identify changes in OH have thus been proposed, including: the concentration of formaldehyde [Staffelbach et al., 1991]; the concentrations of hydrogen peroxide and methyl-peroxide [Gillet et al. 2000]; and the mass-independent fractionation of oxygen isotopes in sulfates [Savarino et al., 2003]. Studies taking a top-down approach implicitly assume the concentration, or isotopic composition, of a constituent trapped or dissolved in the ice bears some relation to the concentration, or isotopic composition, of that constituent in the boundary layer during the period in which gases could freely exchange between the atmosphere and the then un-compacted snow, or 'firn'. In the case of methane, its concentration in air trapped in the ice is almost identical to its concentration in the atmosphere. However, the relationship can be considerably more complicated, as is the case for formaldehyde, the concentration of which in ice is modified during and post-deposition [Hutterli et al., 1999, 2002].

In contrast to previous studies, we take a 'bottom-up' approach, using the Cambridge parallelised-Tropospheric Offline Model of Chemistry and Transport (p-TOMCAT), which is described in Section 2.1, to explore changes in the chemical composition of the Antarctic boundary layer

accompanying source- and sink-driven changes in methane. We carry out six experiments: a PI model run, which is described in Section 2.2, and five sensitivity experiments derived from this, which are described in Section 2.3. Note that we are not trying to simulate the LGM-PI change in methane. Instead, these are highly idealized experiments, exploring extreme scenarios, in an effort to identify any chemical signal (a chemical species, or combination of species, amongst those included in p-TOMCAT) that shows potential to constrain the cause(s) of this change. We examine the results of these experiments in Sections 3.1 and 3.2. In Sections 3.3 and 3.4, we briefly assess the sensitivity of our results to inter-annual variations in meteorology and the definition of the Antarctic boundary layer, respectively, before discussing in Section 4 the preservation in Antarctic ice of those signals which show some potential, and issues surrounding their interpretation.

2 Method

2.1 The Cambridge p-TOMCAT model

For the purposes of this study, we use the Cambridge p-TOMCAT model of tropospheric chemistry and transport, which has been used in a variety of recent studies [Köhler et al., 2008; Yang et al., 2008; Cook et al., 2007; and Levine et al., 2007]. This is a three-dimensional Eulerian model driven by wind, temperature and humidity fields taken from the operational analyses of the European Centre for Medium-range Weather Forecasts (ECMWF). Here, the model is run at a horizontal resolution of approximately 2.8° x 2.8° on 31 levels, which stretch from the surface to 10 hPa with a typical spacing of about 100m in the boundary layer and 1-1.5km in the vicinity of the tropopause. Tracer advection is calculated with the second-order moments advection scheme of Prather [1986], as implemented by Chipperfield [1996]. Transport in the horizontal is driven directly by the ECMWF winds whilst vertical transport is calculated based on the convergence/divergence of winds in the horizontal. Strong convergence also triggers convection, which is simulated using the mass flux parameterization of Tiedtke [1989]. The model also contains a non-local vertical diffusion scheme for the boundary layer based on the parameterization of Holtslag and Boville [1993]; see Wang et al. [1999] for details of its implementation.

The model chemistry includes 52 chemical species and 174 reactions, which describe the gas-phase HO_x/NO_x chemistries of methane, ethane, propane and isoprene, the latter according to the Mainz Isoprene Mechanism [Pöschl et al., 2000]; the model also includes a simple ethene-like tracer, which is simply emitted, and removed by OH. The chemistry scheme is of medium complexity, comparable with the schemes employed in other tropospheric chemistry-transport models, such as the troposphere-only version of the UK Chemistry Aerosol Community Model currently under development (see http://www.ukca.ac.uk), and is suitable for global integrations spanning years to

decades. The bimolecular and termolecular reaction-rate coefficients (last updated in March 2005) are taken from the International Union of Pure and Applied Chemistry [Atkinson et al., 2005] and the Master Chemical Mechanism (see http://mcm.leeds.ac.uk/MCM/home.htt), whilst the photolysis rates are calculated offline using the Cambridge 2D model [Law and Pyle, 1993], which is also used to provide top-boundary conditions for ozone and NO_y. The concentrations of species are integrated forward in time using the ASAD code of Carver et al. [1997] and the IMPACT time integrator of Carver and Stott [2000]. The wet deposition of soluble species is linked to the parameterization of convection (and large-scale rainfall) according to Walton et al. [1988]. The dry deposition of species at the surface is calculated using prescribed 1m deposition velocities [Valentin, 1990], extrapolated to the centre of each grid box in the lowest level of the model according to Berntsen and Isaksen [1997]. For more details on the implementation and validation of the wet- and dry deposition schemes, see Giannakopoulos et al. [1999].

The model does not include halogen chemistry (including the oxidation of methane initiated by atomic chlorine), snow photochemistry or the loss of methane to soils. Platt et al. [2004] estimate that atomic chlorine is responsible for about 3% of global methane loss. We would not expect the inclusion of an additional sink of this size to alter our findings significantly, particularly those of a qualitative nature. Snow photochemistry will affect OH in the boundary layer in snow-covered regions [see, e.g., Grannas et al., 2007]. We would have to include this if our aim was to reproduce absolute OH concentrations measured in such regions, but it should not have much effect on the global oxidizing capacity. Lastly, the loss of methane to soils is omitted on the basis that it accounts for only 5-10% of global methane loss, which is small compared to the uncertainty in the PI emissions of methane implemented in the model [Valdes et al., 2005]; see next section.

2.2 The PI model run

For the purposes of this experiment, we have implemented as far as practically possible the same PI emissions in the Cambridge p-TOMCAT model as Valdes et al. [2005] used in the STOCHEM atmospheric chemistry-transport model. The emissions, summarized in Table 1, include: seasonally varying emissions of nitrogen dioxide (NO_2), methane (CH_4), carbon monoxide (CO), ethane (C_2H_6), propane (C_3H_8), acetone (CH_3COCH_3), isoprene (C_5H_8) and ethene (C_2H_4), in addition to constant emissions of formaldehyde (HCHO) and acetaldehyde (CH_3CHO). Note that, unlike Valdes et al. [2005], we do not include emissions of butane, propene, methanol or α-pinene, owing to the lack of these species in p-TOMCAT; hydrogen is not emitted but is included in the model as a constant field. Lightning emissions of NO_2 in p-TOMCAT are coupled in time and space to the parameterization of convection [Stockwell et al., 1999], and are therefore unlikely to be distributed in the same way, either spatially or temporally, as the lightning emissions of NO in STOCHEM. We note, however, that the total amount of NO_x emitted from lightning in p-TOMCAT (normalized to 4.8 Tg N/year) is not dissimilar to that in STOCHEM (4.2 Tg N/year) [Valdes et al., 2005].

Figure 1 illustrates the distributions of these emissions (excluding lightning emissions of NO_x), integrated over a year. The emissions of methane are dominated by emissions from wetlands in equatorial South America and Indonesia, and to a lesser extent, Central Africa and South East Asia. The relatively small amounts of methane coming from the oceans, biomass burning and termites (see Table 1) account for its near-ubiquitous, low-level emissions elsewhere around the globe. The emissions of isoprene, which exert a strong influence on OH as a result of isoprene's short lifetime with respect to oxidation [Atkinson et al., 2005], are concentrated in equatorial regions, but also appreciable in the sub-tropics of both hemispheres. The remaining emissions categorized under 'vegetation' in Table 1 are all distributed in the same way as each other, mostly in the tropics and sub-tropics but with a significant contribution from mid-latitudes, particularly in the northern

hemisphere. This distribution closely resembles the distribution of acetone emissions, the latter being overwhelmingly dominated by emissions from vegetation (see Table 1).

The PI model run (and each sensitivity experiment) follows a certain format. The model is first run to equilibrium using repeated meteorology from a single year (1997). At 'equilibrium', neither the global burden of methane nor the annual-mean concentration of methane in the Antarctic boundary layer (AntBL; defined to comprise all boxes in the lowest level of the model south of 70°S) changes by more than 0.02% per year. The model is then run with meteorology from three further years (1998-2000) to explore inter-annual variability. These three years were chosen on the basis that they include contrasting phases of the El Niño Southern Oscillation (ENSO), a major contributor to inter-annual variations in the distributions of trace gases within the troposphere [e.g. Chandra et al., 1998; Ziemke and Chandra, 2003]; the northern hemisphere winters of 1997/1998 and 1998/1999 were El Niño and La Niña respectively, whilst 2000 was less affected by the ENSO. The data gathered in these three years are then used to characterize the chemical composition of the AntBL. Note, we assume recent meteorological analyses adequately represent the meteorology of the PI.

2.3 The sensitivity experiments

We carry out five sensitivity experiments, each starting from the PI model setup; these are schematically illustrated in Figure 2. The first two experiments, Sink 1 and Source 1, are designed to identify any chemical signal that responds in a substantially different manner to purely source-driven and purely sink-driven changes in methane (of the same size), making no assumptions about the cause(s) of the latter. In Source 1, we reduce the concentration of methane in the AntBL to roughly that which was present at the LGM by scaling down the emissions of methane (uniformly) by 45%. In Sink 1, we increase the production of OH by a factor of 2.5 to effect the same change in

253 methane concentration. We do so by increasing the number of OH radicals produced as each
254 excited oxygen atom, $O(^1D)$, reacts with a water molecule. This is simply a way of increasing the
255 concentration of OH without making any assumptions about the cause of this increase, which would
256 have chemical consequences. For example, if we were to instead increase the rate of this reaction,
257 we would not only increase the rate of OH formation, but also the rate of $O(^1D)$ removal. The third
258 and fourth experiments, Sink 2 and Source 2, are designed to assess whether there exists a signal
259 capable of differentiating between source- and sink-driven changes in methane, when the latter are
260 the result of changes in the amount of NMVOCs emitted from vegetation. In Sink 2, all emissions
261 from vegetation (i.e. those categorized under 'vegetation' in Table 1) are switched off, leading to a
262 substantial reduction in methane, but a smaller one than in Sink 1 or Source 1. The same reduction
263 in methane is achieved in Source 2, as in Sink 2, by scaling down the emissions of methane by
264 17%. In the fifth experiment, Sink+Source, we remove all emissions from vegetation (as in Sink 2)
265 and scale down the emissions of methane by 31% to reduce the concentration of methane to that
266 which was present at the LGM (as in Sink 1 and Source 1). By comparing the results to this
267 experiment with those to Source 1, we can assess a signal's ability to differentiate between a purely
268 source-driven change in methane, and one which is part source-driven, part sink-driven.
269
270 Though we explore in Sink 1 the consequences of a change in OH generated in such as way as to
271 make no assumptions about the cause(s) of this change, we do not explore changes in OH driven
272 explicitly by changes in NO_x emissions or climate, which would have influences on the atmospheric
273 composition besides their effects on OH, and presumably different ones to the changes in NMVOC
274 emissions that we explore in Sink 2 and Sink+Source. As outlined in Section 1, there are
275 significant uncertainties associated with the changes in NO_x emissions and climate between the
276 LGM and the PI, and their influences on the oxidizing capacity were probably subsidiary to the
277 influence of changes in NMVOC emissions. Our approach is therefore to first try to find a signal
278 capable of differentiating between source- and sink-driven changes in methane, subject to constant

279 NO_x emissions and climate, and only if we find such a signal (and believe it will be preserved in the
280 ice record on the necessary timescales), explore whether it would prove robust to such changes.

3 Results

3.1 Methane in the Antarctic (and Arctic) boundary layer

Figure 3 illustrates the concentrations of methane in the AntBL and the Arctic boundary layer (ArcBL; defined to comprise all boxes in the lowest level of the model north of 70°N) that we calculate in the PI model run (top panel) and the five sensitivity experiments: Sink 1, Source 1 and Sink+Source (bottom panel); Sink 2 and Source 2 (middle panel). In each case, the data correspond to the last three years of the model's run to equilibrium, using repeated 1997 meteorology, and the subsequent three years employing meteorology from 1998-2000.

The PI model run (top panel) yields methane concentrations of 705-720 ppbv in the AntBL and 740-755 ppbv in the ArcBL, amounting to annual-mean concentrations, averaged over 1998-2000, of 709 ppbv and 744 ppbv respectively. (From here on, all annual-mean concentrations refer to averages over 1998-2000.) There is thus an average inter-hemispheric gradient of 35 ppbv, which arises as a result of a bias in the distribution of methane sources towards the northern hemisphere. This compares well with the average inter-hemispheric gradient of 35 (+/-7) ppbv evident from high-resolution measurements between 0.25 and 1ka before present [Chappellaz et al., 1997]. In both the AntBL and the ArcBL, the concentration of methane exhibits an annual cycle, between a maximum in local spring and a minimum in local autumn, with a peak-to-peak amplitude of roughly 10 ppbv. This cycle reflects seasonal variations in the strength of methane emissions. Note that almost identical cycles are calculated in the last three years of the run to equilibrium (3 x 1997), confirming the model had indeed reached equilibrium before it was run with 1998-2000 meteorology. In the latter three years, the concentrations of methane show some inter-annual variability but no obvious trend; we note that the influence of inter-annual variations in meteorology on the concentration of methane has previously been explored by Warwick et al. [2002].

The annual-mean concentration of methane in the AntBL is reduced to around 340 ppbv in Sink 1, Source 1 and Sink+Source (bottom panel). Recall, the aim in these experiments was to reduce the concentration of methane in this region to roughly that which characterized the LGM (~360 ppbv). However, the concentration of methane in the ArcBL is reduced to different extents in these experiments: to 375 ppbv in Sink 1 and around 360 ppbv in Source 1 and Sink+Source. It follows that, relative to the PI, the inter-hemispheric gradient remains unchanged in Sink 1 but is reduced in Source 1 and Sink+Source to around 20 ppbv—a reduction of 43%. It would therefore appear that, in Source 1, the inter-hemispheric gradient scales linearly with the amount of methane emitted, the latter being reduced by 45% relative to the PI. However, this scaling results from the way in which the emissions are reduced; by scaling the emissions uniformly, we do not change their geographical distribution. In reality, the reduction in methane emissions occurred mostly in the northern mid- and high latitudes [e.g. Chappellaz et al., 1993b; Kaplan, 2002], and measurements at the LGM (16.7-20.3ka before present) reveal an inter-hemispheric gradient of only a few ppbv [Dällenbach et al., 2000].

In Sink 2 (middle panel), switching off all emissions from vegetation reduces the annual-mean concentration of methane in the AntBL to 554 ppbv. This reduction equates to just less than half the change in methane observed between the LGM (~360 ppbv) and the PI (~700 ppbv). A similar reduction in AntBL methane is achieved in Source 2 (middle panel) by reducing the emissions of methane by 17%. Meanwhile, the concentration of methane in the ArcBL is reduced to 585 ppbv in Sink 2 and 581 ppbv in Source 2, giving inter-hemispheric gradients of 31 ppbv and 29 ppbv respectively. As before, in Source 2, the gradient in methane scales linearly with the amount of methane emitted because the emissions of methane are scaled uniformly.

3.2 Chemical sensitivities in the AntBL

Table 2 gives the annual-mean concentration of each chemical species in the AntBL, calculated in the PI model run, and the percentage change in this, calculated in each sensitivity experiment. Strictly, the annual-mean PI concentration ($[X]_{PI}$) is the mean of three annual-mean concentrations corresponding to the three years of meteorology (1998-2000) with which the model is driven. Likewise, each percentage change in concentration (e.g. $\Delta[X]_{Sink1\text{-}PI}$) is the mean of three percentage changes in annual-mean concentration (relative to the PI), each subject to a different year's meteorology. The corresponding standard deviations are also given in Table 2. The species in Table 2 are listed in order of the difference between the percentage changes in concentration, or 'sensitivities', they exhibit in Sink 1 and Source 1 (i.e. $|\Delta[X]_{Sink1\text{-}PI} - \Delta[X]_{Source1\text{-}PI}|$).

In the AntBL, OH shows the greatest difference in sensitivity between the first pair of sensitivity experiments, increasing by 112% in Sink 1 and 19% in Source 1 (relative to the PI); the global tropospheric burden of OH increases by 84% in Sink 1 and 12% in Source 1. However, owing to its high reactivity as a radical species, OH will not be preserved in the ice record; hence the need for this study. We can similarly discount all other radical species (not shown in Table 2), and those species which are rapidly broken down into radicals (HONO and N_2O_5), from our list of potential chemical signals. Note that increasing the concentration of OH in Sink 1, by increasing the production of OH, reduces the concentration of methane, whilst reducing the concentration of methane in Source 1 and Source 2, by reducing the amount of methane emitted, increases the concentration of OH—in the AntBL, by 19% and 7% respectively; the global tropospheric burden of OH increases by 12% and 5%. OH and methane thus exhibit an inter-dependence that limits the extent to which we can separately explore the effects of changes in OH/methane emissions. This inter-dependence also constitutes a small positive feedback that reinforces any change we make to OH or methane [Prather, 1996], evidenced by the slightly greater-than-linear reductions in AntBL

359 methane in Source 1 and Source 2, of 52% and 22% respectively, in response to 45% and 17%
360 reductions in methane emissions. (Here, the feedback comprises a reduction in methane lifetime
361 due to an increase in OH, as seen in previous theoretical studies [e.g. Isaksen and Hov, 1987].)
362
363 Isoprene (C_5H_8) and a number of its degradation products (ISON, NALD, MACR, ISOOH, MPAN
364 and HACET) show substantially different sensitivities in Sink 1 and Source 1, decreasing by 50-
365 70% and 10-20% respectively. The 'lumped species' (indicated by parentheses in Table 2), used to
366 describe the oxidation of isoprene in the Mainz Isoprene Mechanism [Pöschl et al., 2000], could in
367 principle provide useful chemical signals, so long as all their (major) constituents are preserved in
368 the ice. However, owing to the negligible concentrations these species exhibit in the PI AntBL,
369 these percentage changes equate to changes in concentration that would be very difficult to detect.
370 Note that the concentration of isoprene, and that of each species derived exclusively from its
371 oxidation, decreases by 100% in Sink 2 and Sink+Source because the emissions from vegetation,
372 which comprise the only source of isoprene in the model, are removed in these experiments.
373
374 Ethane (C_2H_6), ethene (C_2H_4) and propane (C_3H_8) show substantially different sensitivities in Sink
375 1 and Source 1, decreasing by 50-60% and 10-15% respectively. Furthermore, these percentage
376 changes equate to non-negligible changes in concentration, of between 1 and 10 pptv. However,
377 just as it is difficult to differentiate between changes in methane emissions and changes in OH, so it
378 would be difficult to differentiate between changes in the sources and sinks of these hydrocarbons,
379 since oxidation by OH also comprises their main sink. To infer changes in OH from changes in
380 their concentrations, we would need to know if and how their emissions had changed between the
381 LGM and the PI.
382
383 Carbon monoxide (CO) exhibits a moderate difference in sensitivity in the first pair of experiments,
384 decreasing by 56% in Sink 1 and 26% in Source 1. Furthermore, these percentage changes equate

385 to sizeable changes in concentration, of the order of 10 ppbv. However, since its concentration
386 changes in the same sense (decreases) in both experiments, a change in its concentration could not
387 be attributed unambiguously to a particular factor affecting methane, in the absence of additional
388 information. Also, the production of CO within the snow-pack as a result of the photochemical
389 decomposition of other organic species, such as peroxides and formaldehyde, could complicate the
390 interpretation of changes in CO preserved in the ice record [see, e.g., Haan et al., 2001]. It is
391 possible, however, that some information regarding the cause of the LGM-PI change in methane
392 could be gleaned from measurements of the mass-independent fractionation of oxygen isotopes in
393 CO, $\Delta^{17}O_{CO} = \delta^{17}O_{CO} - 0.52\ \delta^{18}O_{CO}$. Measurements indicate that CO exhibits $\Delta^{17}O_{CO}=0$ at the point
394 of emission from a variety of CO sources including biomass burning [Huff and Thiemens, 1998],
395 but increasingly positive $\Delta^{17}O_{CO}$ values downstream that, based on the work of Röckmann et al.
396 [1998b], are attributable to the oxidation of CO by OH. In Section 4, we will discuss what potential
397 there is to infer any change in oxidizing capacity that took place between the LGM and the PI from
398 measurements of $\Delta^{17}O_{CO}$ performed on CO trapped in polar ice.
399
400 Hydrogen peroxide (H_2O_2) is the only non-radical species whose concentration appears to change in
401 an opposite sense (i.e. either increases or decreases) depending on the cause of the change in
402 methane, increasing in Sink 1 by 8% and decreasing in Source 1 by 16%. Although small, these
403 percentage changes equate to non-negligible changes in concentration, of the order of 10 pptv. We
404 note, however, that H_2O_2 decreases in Sink 2, Source 2 and Sink+Source, by 38%, 7% and 46%
405 respectively. It will therefore be less useful in differentiating between changes in methane
406 emissions and changes in OH, if the latter are driven by changes in emissions from vegetation; we
407 would be reliant on inferring something from the magnitude of the change in H_2O_2 concentration.
408
409 Peroxy acetyl nitrate (PAN) shows only a modest difference in sensitivity, decreasing by 30% in
410 Sink 1 and 1% in Source 1. However, the lack of sensitivity that PAN shows to changes in methane

411 emissions (confirmed in Source 2) could make it a useful indicator of changes in OH. We note that
412 PAN shows a particularly strong sensitivity to changes in the emissions from vegetation, decreasing
413 by 98% in Sink 2 and Sink+Source. This presumably reflects the near-complete removal of
414 NMVOCs (see Table 1) from which CH_3CO_3 radicals, which combine with NO_2 to form PAN, are
415 derived. We would similarly expect PAN to change in response to changes in NO_x emissions.
416 Changes in climate could also affect PAN, by altering its lifetime with respect to thermal
417 decomposition. We have not, however, explored these additional sensitivities. In Section 4, we
418 will discuss the likelihood that PAN is preserved in the ice record.
419
420 Formaldehyde (HCHO) also shows a modest difference in sensitivity, decreasing by 11% in Sink 1
421 and 40% in Source 1. However, the value previously recognized in HCHO [see Staffelbach et al.,
422 1991] lies in its close relationship with methane and OH. Assuming a steady state between HCHO
423 production by methane oxidation and HCHO loss by photolysis and reaction with OH, Staffelbach
424 et al. [1991] proposed a formula to relate the concentrations of HCHO, methane and OH in remote
425 regions (i.e. far from HCHO sources): equation 1, where k_1 and k_2 are the rate coefficients for the
426 oxidation by OH of methane and HCHO, respectively, and k_p is the J-value for HCHO photolysis.
427
428 $$[HCHO] = \frac{k_1.[OH].[CH_4]}{k_p + k_2.[OH]} \quad \text{that rearranges to} \quad [OH] = \frac{k_p.[HCHO]}{k_1.[CH_4] - k_2.[HCHO]} \qquad (1)$$
429
430 Staffelbach et al. [1991] went on to suggest that contemporaneous measurements of HCHO and
431 methane could be used to estimate past OH concentrations. To test the proposed relationship
432 between atmospheric HCHO, methane and OH, we have calculated how we would expect AntBL
433 OH to change in each sensitivity experiment based on the modeled changes in AntBL HCHO and
434 methane. These are compared with the modeled changes in AntBL OH (previously shown in Table

435 2) in Table 3. For these calculations, we have used the same rate coefficients (k_1 and k_2) as used in
436 the model, subject to the model's annual-mean AntBL temperature (246K in 1998, 1999 and 2000).
437
438 It would appear that reasonable estimates of changes in AntBL OH can be obtained from known
439 changes in AntBL HCHO and methane; the discrepancies are likely to be at least partly attributable
440 to the production of HCHO via NMVOC oxidation, which is not included in equation 1, and the
441 transport of HCHO into, and out of, the AntBL. The change in the concentration of OH in the
442 AntBL may, however, be of limited use in inferring the cause of a change in methane, as OH in the
443 AntBL will not be representative of OH at low latitudes (i.e. between 30°N and 30°S), where most
444 methane is oxidized [see, e.g., Lawrence et al., 2001; Labrador et al., 2004]. This is most evident
445 from the results of Sink 2, in which the removal of emissions from vegetation (concentrated at low
446 latitudes; see Figure 1) leads to a 13% increase in the concentration of OH in the AntBL but a 28%
447 increase in the global tropospheric burden of OH. Additionally, the relationship proposed by
448 Staffelbach et al. [1991] does not appear to be capable of differentiating between a purely source-
449 driven change in methane, and one which is part source-driven, part-sink driven; using equation 1,
450 we estimate a greater increase in AntBL OH in Source 1 than in Sink+Source, but the model shows
451 the reverse (Table 3). We will, nevertheless, discuss HCHO further in Section 4.
452
453 Most of the remaining species show small differences in sensitivity, and hence little potential to
454 provide useful chemical signals. However, one such species, ozone (O_3), warrants further attention,
455 as does H_2O_2 (already mentioned), in light of the large difference in sensitivity OH exhibits, and the
456 link identified by Savarino et al. [2000] between the relative importance of different S(IV)-
457 oxidation pathways and the mass-independent fractionation of oxygen isotopes in sulfates,
458 $\Delta^{17}O_{sulfates} = \delta^{17}O_{sulfates} - 0.512\ \delta^{18}O_{sulfates}$. According to Savarino et al. [2000], $\Delta^{17}O_{sulfates}$ is
459 attributable to the transfer of $\Delta^{17}O$ anomalies in tropospheric O_3 and H_2O_2, 31‰ [Johnston and
460 Thiemens, 1997] and 1.7‰ [Savarino and Thiemens, 1999] respectively, to sulfates as they oxidize

461 sulfur dioxide (SO_2) in the aqueous phase; OH exhibits near-zero $\Delta^{17}O$ anomalies in the troposphere
462 [Lyons, 2001], and no anomaly is transferred as it oxidizes SO_2 in the gas phase [Savarino et al.,
463 2000]. All else being equal, therefore, a change in the relative concentrations of OH, O_3 and H_2O_2,
464 where the SO_2 is oxidized, should to lead to a change in $\Delta^{17}O_{sulfates}$. Given the large $\Delta^{17}O$ anomaly
465 in O_3, $\Delta^{17}O_{sulfates}$ will be most sensitive to changes in the $[O_3]/[OH]$ and $[O_3]/[H_2O_2]$ ratios. Table 4
466 gives the percentage changes in these ratios in the AntBL, based on the changes in annual-mean
467 OH, O_3 and H_2O_2 concentrations calculated in each sensitivity experiment.
468
469 The $[O_3]/[OH]$ ratio decreases in all five sensitivity experiments. All else being equal, this should
470 lead to a reduction in the $\Delta^{17}O$ in sulfates formed in the AntBL. However, with the exception of
471 Sink 1, in which we artificially increase the strength of the OH source, the $[O_3]/[H_2O_2]$ ratio
472 increases in each experiment, tending to increase the $\Delta^{17}O$ in the sulfates formed here. As we do
473 not know what proportions of SO_2 were oxidized by OH, O_3 and H_2O_2 in the PI AntBL, we cannot
474 say what the net effect of these changes would be, and it remains to be seen what difference in
475 sensitivity $\Delta^{17}O_{sulfates}$ shows to changes in OH/methane emissions. These proportions could be
476 estimated using a general circulation model with interactive aerosol dynamics and appropriate
477 chemistry, such as that employed by Cosme et al. [2002] in the Laboratoire de Meteorologie
478 Dynamique-Zoom Tracers model, as could the influence the $\Delta^{17}O$ in sulfates formed upwind of the
479 AntBL has on the $\Delta^{17}O_{sulfates}$ in this region. However, to accurately model, not only the
480 distributions of SO_2, OH, O_3 and H_2O_2, but also that of liquid water (necessary for SO_2-oxidation in
481 the aqueous phase), and the transport of air to the AntBL, would pose a formidable challenge. With
482 this in mind, we will discuss in Section 4 what potential the $\Delta^{17}O_{sulfates}$ preserved in Antarctic ice
483 [see, e.g., Alexander et al., 2002; Savarino et al., 2003] has to constrain the cause of the LGM-PI
484 change in methane.
485
486

3.3 Inter-annual variability in meteorology

Until now, we have only examined annual-mean concentrations, and percentage changes therein, averaged over three model years. However, since the three model years employ different meteorological analyses, we have an opportunity to explore inter-annual variations in the chemical composition of the AntBL resulting from changes in meteorology, specifically to assess whether or not the chemical sensitivities described in the previous section prove robust to these. Table 2 gives the mean sensitivity exhibited by each species in each of the five sensitivity experiments and their standard deviations. The sensitivities exhibited by the majority of species show little variability, their standard deviations being equivalent to around 10% of their mean values, or less. Those exhibited by HONO, $HONO_2$ and N_2O_5 show greater variability, as do those of C_5H_8, PPAN and a number of radical species (not shown in Table 2). However, importantly, none of the sensitivities exhibited by species contributing to potentially useful chemical signals (PAN, HCHO, OH, O_3 or H_2O_2) show much variability: they prove robust to inter-annual changes in meteorology.

3.4 The definition of the AntBL

The model's ability to capture the structure of the AntBL, particularly its shallow depth under stable conditions [Davis et al., 2004; Anderson and Neff, 2008], is limited by the vertical resolution of the model, the lowest level being at least 100m deep, and the quality of the meteorological analyses with which it is driven; see Section 2.1 for more details on the model. Recall, for the purposes of this study, the AntBL was simply defined to comprise all grid boxes in the lowest level of the model, located south of 70°S. To assess how sensitive our results are to this somewhat arbitrary definition, we have repeated our analysis using two alternative definitions, comprising: all grid boxes in the second lowest level of the model south of 70°S; and all grid boxes in the lowest level

513 of the model south of 80°S. Subject to each definition, we calculate a slightly different (area-
514 weighted) average AntBL concentration for each species in the PI model run and each sensitivity
515 experiment (not shown). Importantly, however, the percentage change in concentration that each
516 species shows in each sensitivity experiment, relative to the PI, changes very little—by a few
517 percent, at most. The chemical sensitivities described in Section 3.2 thus prove insensitive to the
518 precise definition of the AntBL employed.

4 Summary and Discussion

4.1 Summary

Using an atmospheric chemistry-transport model, we have explored the effects of source- and sink-driven changes in methane on a wide range of chemical species in the AntBL. Our aim has been to identify any atmospheric chemical signals that, provided they are preserved in the ice record on the necessary timescales, could help us to differentiate between the source- and sink-driven components of the increase in methane between the LGM and the PI [Loulergue et al., 2008]. The majority of species have been discounted on the basis that: they show too similar sensitivities to changes in OH/methane emissions; they are too reactive to be preserved in the ice on the necessary timescales (e.g. radical species); they exhibit negligible concentrations in the PI AntBL (e.g. isoprene and its oxidation products); and/or additional, unknown information is required to interpret changes in their concentrations, such as if and how their source strengths have changed (e.g. other hydrocarbons). Four signals, however, warrant further discussion regarding their preservation in Antarctic ice and issues surrounding their interpretation: the concentration of PAN; the mass-independent fractionation of oxygen isotopes in sulfates, $\Delta^{17}O_{sulfates}$, and CO, $\Delta^{17}O_{CO}$; and the concentration of HCHO.

4.2 PAN: short-term preservation in the Antarctic-ice record

Based on our calculations, changes in the concentration of PAN in the AntBL could be indicative of changes in OH and/or changes in NMVOC emissions from vegetation—a potential driver of changes in OH. We note, however, that the concentration of PAN would also be affected by

544 changes in NO_x emissions and temperature, which have not been explored; see Section 3.2 for more
545 details.
546
547 In theory, PAN could be preserved in the ice record in either the gas phase (in air bubbles trapped
548 within the ice) or in aqueous solution (within the ice itself). As a result of wind-pumping and/or
549 rapid accumulation, gaseous PAN could quickly reach depths in the snowpack to which light does
550 not penetrate. Here, photolysis and oxidation by OH will cease, however, thermal decomposition
551 and dissolution will continue. Based on the kinetic data of Bridier et al. [1991], we estimate that the
552 lifetime of PAN with respect to thermal decomposition will vary between about a week in summer
553 (assuming a temperature of 265K) and roughly a decade in winter (assuming a temperature of
554 235K). It is therefore unlikely that PAN will survive in the gas phase for more than, at most, 30-40
555 years (3-4 e-folding lifetimes). According to Kames and Schurath [1995], that which survives
556 decomposition, but instead undergoes dissolution, will be hydrolyzed on timescales of the order of
557 an hour. We conclude that PAN will not be preserved, either in the gas phase or in aqueous
558 solution, on the timescales necessary to explore changes in OH/methane emissions between the
559 LGM and the PI.
560
561
562 **4.3 $\Delta^{17}O_{sulfates}$: limited potential to constrain the cause of the LGM-PI change in methane**
563
564 Samples from the Vostok ice core (East Antarctica) indicate that $\Delta^{17}O_{sulfates}$ was about 2‰ lower
565 during the last glacial period (~60ka before present) than in the early Holocene (~10ka before
566 present) [Alexander et al., 2002]. The question is, what can we infer from this regarding the cause
567 of the change in methane between the LGM and the PI? Alexander et al. [2002] primarily attribute
568 the change in $\Delta^{17}O_{sulfates}$ to a change in the relative concentrations of OH, O_3 and H_2O_2 in the
569 troposphere, and/or a change in cloud-processing efficiency (i.e. the availability of liquid water for

570 aqueous-phase SO_2-oxidation), but identify a number of other factors that could have also affected
571 $\Delta^{17}O_{sulfates}$: the fraction of sulfates from primary sources, which exhibit $\Delta^{17}O=0$ and thus dilute non-
572 zero $\Delta^{17}O_{sulfates}$; the pH of water droplets in the atmosphere, which affects the amount of SO_2
573 oxidized by O_3, as opposed to H_2O_2, in the aqueous phase [Seinfield and Pandis, 1998]; and the
574 dynamics of the troposphere, which govern the transport of air to the Vostok site. Even if these
575 additional factors could be discounted, or their effects on $\Delta^{17}O_{sulfates}$ accurately quantified, it would
576 still be very difficult to deduce, quantitatively, how the relative concentrations of OH, O_3 and H_2O_2
577 changed during the glacial-interglacial transition, this being convolved with the influence of any
578 change in cloud-processing efficiency that accompanied the change in climate.
579
580 The only way we can see of quantitatively exploring how changes in the relative concentrations of
581 these oxidants may have contributed to the change in $\Delta^{17}O_{sulfates}$ is to use a general circulation
582 model with interactive aerosol dynamics and appropriate chemistry to simulate $\Delta^{17}O_{sulfates}$, subject
583 to a variety of meteorological and trace-gas emissions scenarios. Verma et al. [2007] used such a
584 model to explore the present-day atmospheric sulfur budget, finding OH, O_3 and H_2O_2 to be
585 responsible, annually, for 29%, 30% and 41% of SO_2-oxidation globally; see Benkovitz et al.
586 [2006] and Berglen et al. [2004] for similar calculations. Using existing knowledge of the $\Delta^{17}O$
587 anomalies in tropospheric O_3 and H_2O_2 [Johnston and Thiemens, 1997; Savarino and Thiemens,
588 1999], the transfer of these to sulfates via SO_2-oxidation [Savarino et al., 2000], and the dilution of
589 these by the mixing-in of primary sulfates [see, e.g., Alexander et al., 2002], the $\Delta^{17}O_{sulfates}$ at the
590 Vostok site could be simulated; such an approach has been taken to quantitatively interpret recent
591 observations of $\Delta^{17}O_{sulfates}$ in the Indian Ocean marine boundary layer, and at the Alert station in the
592 Arctic [see Alexander et al., 2005, 2009]. It is unlikely, however, that only one
593 meteorological/trace-gas emission scenario would be found that could account for the reduction in
594 $\Delta^{17}O_{sulfates}$ during the glacial period (to within the uncertainty of the measurements); recall, we
595 found that the $[O_3]/[OH]$ and $[O_3]/[H_2O_2]$ ratios, at least in the AntBL, responded in the same sense

596 to an increase in OH (driven by a reduction in NMVOC emissions from vegetation) and/or a
597 reduction in methane emissions; see Section 3.2. Furthermore, given the lifetime of sulfate aerosol,
598 $\Delta^{17}O_{sulfates}$ in Antarctic ice could reflect changes in oxidative conditions over much of the Southern
599 Ocean, but is unlikely to tell us much about changes in OH at low latitudes, where most methane is
600 oxidized [see, e.g., Lawrence et al., 2001; Labrador et al., 2004]. Coupled to the large uncertainties
601 in meteorology and chemistry, to which simulations of $\Delta^{17}O_{sulfates}$ would be subject, we conclude
602 that $\Delta^{17}O_{sulfates}$ has limited potential to constrain the cause of the LGM-PI change in methane.
603
604
605 **4.4 $\Delta^{17}O_{CO}$: some potential to constrain the cause of the LGM-PI change in methane**
606
607 Records of atmospheric CO concentration spanning the last 200 and 2000 years have been obtained
608 from Antarctic and Greenland ice cores [Haan et al., 1996; Haan and Raynaud, 1998]. However, it
609 remains to be seen whether an ice-core record of $\Delta^{17}O_{CO}$ spanning the last 21ka can be obtained,
610 and the extent to which an accurate record of atmospheric $\Delta^{17}O_{CO}$ could be derived from it; any CO
611 produced in the snowpack [see Haan et al., 2001], assuming this exhibits $\Delta^{17}O_{CO}=0$, would dilute
612 the non-zero atmospheric $\Delta^{17}O_{CO}$, and any OH present in the uppermost layer of the snowpack, into
613 which light can penetrate, could continue to alter $\Delta^{17}O_{CO}$. But if we suppose a suitable record of
614 atmospheric $\Delta^{17}O_{CO}$ could be obtained, based on the work of Huff and Thiemens [1998] and
615 Röckmann et al. [1998b], it would contain information on the degree to which CO transported to the
616 ice-core site had been exposed to OH—an average over all air parcels transported to that site,
617 smoothed on the timescale it took sufficient snow to accumulate, and compress under its own
618 weight, to the point of the closure.
619

620 $\Delta^{17}O_{CO}$ has some advantages over $\Delta^{17}O_{sulphates}$, so far as inferring a change in oxidizing capacity is
621 concerned: CO has a much longer lifetime, of the order of weeks to months as opposed to days, and
622 consequently $\Delta^{17}O_{CO}$ should contain more information on OH at low latitudes; and the modeling of
623 $\Delta^{17}O_{CO}$ would not require the modeling of the distribution of liquid water to the same degree of
624 accuracy, since the relevant gas-phase reaction (between CO and OH) is not in direct competition
625 with reactions in the aqueous phase. However, it would not be trivial to infer quantitative changes
626 in OH from changes in $\Delta^{17}O_{CO}$, since the integrated exposure of CO to OH is a function, not only of
627 the OH concentrations present between the source of CO and the site of the ice core, but also the
628 time for which the CO is exposed to those concentrations of OH, which is dependent on two factors
629 that could change with climate: the location of the CO source; and the atmospheric circulation
630 governing its transport to the ice-core site. The changes in $\Delta^{17}O_{CO}$ due to changes in OH would
631 also have to be separated from those due to changes in the amount of CO produced via the
632 ozonolysis of unsaturated hydrocarbons, such as isoprene and terpenes [Röckmann et al., 1998a].
633 We therefore conclude that $\Delta^{17}O_{CO}$ may have some potential to constrain the cause of the LGM-PI
634 change in methane, but further work is needed before this can be fully assessed.
635
636
637 **4.5 HCHO: synchronization of gas- and aqueous-phase Antarctic-ice records**
638
639 Ever since it was proposed by Staffelbach et al. [1991], there has been considerable interest in the
640 use of contemporaneous measurements of HCHO and methane to estimate past OH concentrations.
641 Our calculations confirm that, at least in our model domain, reasonably good estimates of changes
642 in AntBL OH can be obtained from known changes in AntBL HCHO and methane using their
643 formula: equation 1 in Section 3.2. However, we face two problems with regards to using the
644 HCHO preserved in Antarctic ice to determine the cause of the LGM-PI change in methane.
645 Firstly, the concentration of HCHO preserved in the ice differs from that which was present in the

boundary layer, at the time of deposition, as a result of physical processes operating during and post-deposition [Hutterli et al., 1999, 2002]; if we were not focused on the pristine environment of the PI AntBL, we would also have to consider HCHO production within the snowpack [Sumner and Shepson, 1999; Dominé and Shepson, 2002]. The physical processes operate to greater or lesser extents depending on a number of climatic variables: the temperature, the degree to which the snowpack is ventilated, and the rate and seasonality of accumulation. According to Hutterli et al. [2003], the preservation of HCHO is not especially sensitive to changes in ventilation, whilst past temperatures and accumulation rates can be determined from measurements of $\delta^{18}O$ and annual-layer thickness respectively. However, uncertainty surrounding past changes in the seasonality of accumulation make it a formidable challenge to obtain a reliable record of AntBL HCHO during periods of climate change, such as that between the LGM and the PI. The second problem is that even if we were able to obtain a reliable record of AntBL HCHO, and thereby infer a change in AntBL OH, we still would not know if, and how, the oxidizing capacity had changed at lower latitudes, where most methane is oxidized [see, e.g., Lawrence et al., 2001; Labrador et al., 2004].

In one respect, however, the Antarctic-ice record of HCHO does have potential: to synchronize the gas- and aqueous-phase Antarctic-ice records. The gas-phase record includes information regarding past atmospheric CO_2 concentrations, whilst the aqueous-phase record holds information on past changes in temperature ($\delta^{18}O$). Precisely determining the phasing between the changes in CO_2 and temperature requires a synchronization of contemporaneous events in the two records. This has been achieved in Greenland by aligning changes in $\delta^{18}O$ (aqueous phase) and $\delta^{15}N$ (gas phase) accompanying rapid changes in temperature [see, e.g., Severinghaus et al., 1998]. However, the changes in temperature in the Antarctic are not sufficiently rapid to achieve adequate synchronicity, and an alternative signal has yet to be identified. If an aqueous-phase signal could be found that responds to rapid changes in methane preserved in the gas phase, synchronization could be achieved.

672

673 Figure 4 illustrates measurements of methane concentration (blue line) and temperature (relative to
674 the late Holocene; red line) from Dome C, Antarctica, spanning Dansgaard-Oeschger events 7 and 8
675 (roughly 35 and 38ka before 1950); the data are taken from Loulergue et al. [2008] and Jouzel et al.
676 [2007] respectively. The regions shaded grey indicate periods of 200 years at the beginning of
677 these events, in which the concentration of methane increases rapidly by 70-80 ppbv, or 15-20%,
678 whilst the temperature, smoothed on a 200 year timescale (black line), hardly changes. This is in
679 stark contrast to the situation in Greenland, where the rapid changes in methane concentration took
680 place during periods of rapid climate change, which would have influenced the preservation of
681 HCHO in Greenland ice [Fuhrer et al. 1993]. In Antarctica, the slowly varying climate should only
682 lead to modest and smooth variations in HCHO concentration, on top of which each rapid 15-20%
683 rise in methane concentration (recorded in the gas phase) should superimpose a rapid 15-20% rise
684 in HCHO concentration (recorded in the aqueous phase); see equation 1 in Section 3.2. For each
685 such rise in HCHO concentration that could be detected and aligned with the corresponding rise in
686 methane concentration, the gas- and aqueous-phase Antarctic-ice records could be synchronized.
687 The relative phasing of glacial-interglacial changes in CO_2 and temperature in the southern
688 hemisphere could thus be determined. To determine whether CO_2 'led' temperature in this region,
689 or temperature 'led' CO_2, would represent a key step forward in understanding past climate change.
690

691

692 **4.6 Concluding remarks**

693

694 Despite the potentially positive use of HCHO discussed above, our bottom-up model study has not
695 readily identified a chemical signal, likely to be measurable in Antarctic ice cores, that provides a
696 simple and robust constraint on the sizes of the source- and sink-driven changes in atmospheric
697 methane between the LGM and the PI. We have only explored a domain in which NO_x emissions

and climate remain constant. However, given the uncertainties associated with the changes in these factors, we would anticipate their inclusion to make it harder still to identify a robust signal. For the time being at least, we suggest a full understanding of the increase in atmospheric methane between the LGM and the PI will have to rely on a combination of: direct observational constraints on the methane budget in ice cores, such as $\delta^{13}CH_4$ and $\delta D(CH_4)$ [see, e.g., Fischer et al., 2008]; data syntheses leading to improved quantification of changes in methane (and NMVOC) sources [see, e.g., Power et al., 2008]; and comprehensive earth system models with which we can integrate these.

Acknowledgements

This study is part of the British Antarctic Survey Polar Science for Planet Earth Programme and a contribution to the Dynamics of the Earth System and the Ice-core Record project, the latter being jointly funded by the Natural Environment Research Council's programme, Quantifying and Understanding the Earth System, and the French Institut National des Sciences de l'Univers; we gratefully acknowledge their support. The authors also wish to thank: Paul Valdes of the School of Geographical Sciences, University of Bristol, for the PI emissions; Nicola Warwick of the Centre for Atmospheric Science, University of Cambridge, for her help in implementing these emissions in the Cambridge p-TOMCAT model; and three anonymous reviewers for their insightful comments.

719 **References**

720

721 Adams, J. M., J. V. H. Constable, A. B. Guenther, and P. Zimmerman (2001), An estimate of
722 natural volatile organic compound emissions from vegetation since the last glacial maximum,
723 *Chemosphere - Global Change Science*, *3*, 73-91.

724

725 Alexander, B., J. Savarino, N. I. Barkov, R. J. Delmas, and M. H. Thiemens (2002), Climate driven
726 changes in the oxidation pathways of atmospheric sulphur, *Geophys. Res. Lett.*, *29*,
727 doi:10.1029/2002GL014879.

728

729 Alexander, B., J. Savarino, C. C. W. Lee, R. J. Park, D. J. Jacob, Q. Li, R. M. Yantosca, and M. H.
730 Thiemens (2005), Sulfate formation in sea-salt aerosols: Constraints from oxygen isotopes, *J.*
731 *Geophys. Res.*, *110*, doi:10.1029/2004JD005659.

732

733 Alexander, B., R. J. Park, D. J. Jacob, and S. L. Gong (2009), Transition metal-catalyzed oxidation
734 of atmospheric sulfur: Global implications for the sulfur budget, *J. Geophys. Res.*, *114*, D02309,
735 doi:10.1029/2008JD010486.

736

737 Anderson, P. S., and W. D. Neff (2008), Boundary layer physics over snow and ice, *Atmos. Chem.*
738 *Phys.*, *8*, 3563-3582.

739

740 Atkinson, R., D. L. Baulch, R. A. Cox, J. N. Crowley, R. F. Hampson, R. G. Hynes, M. E. Jenkin, J.
741 A. Kerr, M. J. Rossi, and J. Troe (2005), Summary of Evaluated Kinetic and Photochemical Data
742 for Atmospheric Chemistry, Available: http://www.iupac-kinetic.ch.cam.ac.uk.

743

744 Arneth, A., Ü. Niinemets, S. Pressley, J. Bäck, P. Hari, T. Karl, S. Noe, I. C. Prentice, D. Serça, T.
745 Hickler, A. Wolf, and B. Smith (2007), Process-based estimates of terrestrial ecosystem isoprene
746 emissions: incorporating the effects of a direct CO_2-isoprene interaction, *Atmos. Phys. Chem.*, *7*, 31-
747 53.
748
749 Benkovitz, C. M., S. E. Schwartz, M. P. Jensen, and M. A. Miller (2006), Attribution of modeled
750 atmospheric sulfate and SO_2 in the Northern Hemisphere for June-July 1997, *Atmos. Chem. Phys.*,
751 *6*, 4723-4738.
752
753 Berglen, T. F., T. K. Berntsen, I. S. A. Isaksen, and J. K. Sundet (2004), A global model of the
754 coupled sulfur/oxidant chemistry in the troposphere: The sulfur cycle, *J. Geophys. Res.*, *109*,
755 D19310, doi:10.1029/2003JD003948.
756
757 Berntsen, T., K., and I. S. A. Isaksen (1997), A global three-dimensional chemical transport model
758 for the troposphere 1. Model description and CO and ozone results, *J. Geophys. Res.*, *102*, 21,239-
759 21,280.
760
761 Braconnot, P., B. Otto-Bliesner, S. Harrison, S. Joussaume, J.-Y. Peterchmitt, A. Abe-Ouchi, M.
762 Crucifix, E. Driesschaert, Th. Fichefet, C. D. Hewitt, M. Kageyama, A. Kitoh, A. Laîné, M.-F.
763 Loutre, O. Marti, U. Merkel, G. Ramstein, P. Valdes, S. L.Weber, Y. Yu, and Y. Zhao (2007),
764 Results of PMIP2 coupled simulations of the Mid-Holocene and Last Glacial Maximum – Part 1:
765 experiments and large-scale features, *Clim. Past*, *3*, 261-277.
766
767 Bridier, I., F. Caralp, H. Loirat, R. Lesclaux, B. Veyret, K. H. Becker, A. Reimer, and F. Zabel
768 (1991), Kinetic and Theoretical Studies of the Reactions $CH_3C(O)O_2 + NO_2 + M \leftrightarrow$

769 $CH_3C(O)O_2NO_2$ + M between 248 and 393 K and between 30 and 760 Torr, *J. Phys. Chem.*, *95*,
770 3594-3600.
771
772 Carver, G. D., P. D. Brown, and O. Wild (1997), The ASAD atmospheric chemistry integration
773 package and chemical reaction database, *Comput. Phys. Comms.*, *105*, 197-215.
774
775 Carver, G. D., and P. A. Stott (2000), IMPACT: an implicit time integration scheme for chemical
776 species and families, *Ann. Geophys.*, 18,337-18,346.
777
778 Chandra, S., J. R. Ziemke, W. Min, and W. G. Read (1998), Effects of 1997-1998 El Nino on
779 tropospheric ozone and water vapour, *Geophys. Res. Lett.*, *25* (20), 3867-3870.
780
781 Chappellaz, J., T. Bluniert, D. Raynaud, J. M. Barnola, J. Schwander, and B. Stauffert (1993a),
782 Synchronous changes in atmospheric CH4 and Greenland climate between 40 and 8 kyr BP, Letters
783 to Nature, *Nature*, *366*, 443-445.
784
785 Chappellaz, J. A., I. Y. Fung, and A. M. Thompson (1993b), The atmospheric CH_4 increase since
786 the Last Glacial Maximum (1). Source estimates, *Tellus*, *45B*, 228-241.
787
788 Chappellaz, J., T. Blunier, S. Kints, A. Dällenbach, J.-M. Barnola, J. Schwander, D. Raynaud, and
789 B. Stauffer (1997), Changes in the atmospheric CH_4 gradient between Greenland and Antarctica
790 during the Holocene, *J. Geophys. Res.*, *102*, 15,987-15,997.
791
792 Chipperfield, M. P. (1996), The TOMCAT Offline Transport Model, Part II. Dynamics and
793 Advection, UGAMP Internal Report No. 44b, Dep. of Meteorol., Univ. of Reading, Reading, UK.
794

795 Cook, P., N. Savage, S. Turquety, G. Carver, F. O'Connor, A. Heckel, D. Stewart, L. Whalley, A.
796 Parker, H. Schlager, H. Singh, M. Avery, G. Sachse, W. Brune, A. Richter, J. Burrows, R. Purvis,
797 A. Lewis, C. Reeves, P. Monks, J. Levine, and J. Pyle (2007), Forest fire plumes over the North
798 Atlantic: p-TOMCAT model simulations with aircraft and satellite measurements from the
799 ITOP/ICARTT Campaign, *J. Geophys. Res.*, *112*, doi:10.1029/2006JD007563.
800
801 Cosme, E., C. Genthon, P. Martinerie, O. Boucher, and M. Pham (2002), The sulfur cycle at high-
802 southern latitudes in the LMD-ZT General Circulation Model, *J. Geophys. Res.*, *107*, D23, doi:
803 10.1029/2002JD002149.
804
805 Dällenbach, A., T. Blunier, J. Flückiger, B. Stauffer, J. Chappellaz, and D. Raynaud (2000),
806 Changes in the atmospheric CH_4 gradient between Greenland and Antarctica during the last glacial
807 and the transition to the Holocene, *Geophys. Res. Lett.*, *27*, 1005–1008.
808
809 Davis, D., G. Chen, M. Buhr, J. Crawford, D. Lenschow, B. Lefer, R. Shetter, F. Eisele, L.
810 Mauldin, and A. Hogan (2004), South Pole NO_x chemistry: an assessment of factors controlling
811 variability and absolute levels, *Atmos. Environ.*, *38*, 5375–5388.
812
813 Dominé, F., and P. B. Shepson (2002), Air-snow interactions and atmospheric chemistry, *Science*,
814 *297*, 1506-1509.
815
816 Fischer, H., M. Behrens, M. Bock, U. Richter, J. Schmitt, L. Loulergue, J. Chappellaz, R. Spahni,
817 T. Blunier, M. Leuenberger, and T. F. Stocker (2008), Changing boreal methane sources and
818 constant biomass burning during the last termination, *Nature*, *452*, 864-867.
819

820 Fuhrer, K., A. Neftel, M. Anklin and V. Maggi (1993), Continuous measurements of hydrogen
821 peroxide, formaldehyde, calcium and ammonium concentrations along the new GRIP core from
822 Summit, central Greenland, *Atmos. Environ.*, *27A* (12), 1873-1880.
823
824 Giannakopoulos, C., M. P. Chipperfield, K. S. Law, and J. A. Pyle (1999), Validation and
825 intercomparison of wet and dry deposition schemes using Pb-210 in a global three-dimensional off-
826 line chemical transport model, *J. Geophys. Res.*, *104*, 23,761-23,784.
827
828 Gillet, R. W., T. D. Van Ommen, A. V. Jackson, and G. P. Ayers (2000), Formaldehyde and
829 peroxide concentrations in Law Dome (Antarctica) firn and ice cores, *J. Glaciology*, *46*, 152.
830
831 Grannas, A. M., A. E. Jones, J. Dibb, M. Ammann, C. Anastasio, H. J. Beine, M. Bergin,
832 J. Bottenheim, C. S. Boxe, G. Carver, G. Chen, J. H. Crawford, F. Dominé, M. M. Frey,
833 M. I. Guzmán, D. E. Heard, D. Helmig, M. R. Hoffmann, R. E. Honrath, L. G. Huey, M. Hutterli,
834 H. W. Jacobi, P. Klán, B. Lefer, J. McConnell, J. Plane, R. Sander, J. Savarino, P. B. Shepson,
835 W. R. Simpson, J. R. Sodeau, R. von Glasow, R. Weller, E. W. Wolff, and T. Zhu (2007), An
836 overview of snow photochemistry: evidence, mechanisms and impacts, *Atmos. Chem. Phys.*, *7*,
837 4329-4373.
838
839 Haan, D., P. Martinerie, and D. Raynaud (1996), Ice Core Data of Atmospheric Carbon Monoxide
840 Over Antarctica and Greenland During the Last 200 Years, *Geophys. Res. Lett.*, *23*, 2235-2238.
841
842 Haan D., Y. Zuo, V. Gros, and C. A. M. Brenninkmeijer (2001), Photochemical production of
843 carbon monoxide in snow, *J. Atmos. Chem.*, *40*, 217-230.
844

845 Haan, D., and D. Raynaud (1998), Ice core record of CO variations during the last two millennia:
846 atmospheric implications and chemical interactions within the Greenland ice, *Tellus*, *50B*, 253-262.
847
848 Holtslag, A. A. M., and B. A. Boville (1993), Local versus Nonlocal Boundary-Layer Diffusion in a
849 Global Climate Model, *J. Clim.*, *6*, 1825-1842.
850
851 Huff, A. K., and M. H. Thiemens (1998), O-17/O-16 and O-18/O-16 isotope measurements of
852 atmospheric carbon monoxide and its sources, *Geophys. Res. Lett.*, *25*, 3509-3512.
853
854 Hutterli, M. A., R. Röthlisberger, and R. C. Bales (1999), Atmosphere-to-snow-to-firn transfer
855 studies of HCHO at Summit, Greenland, *Geophys. Res. Lett.*, *26* (12), 1691-1694.
856
857 Hutterli, M. A., R. C. Bales, J. R. McConnell, and R. W. Stewart (2002), HCHO in Antarctic snow:
858 Preservation in ice cores and air-snow exchange, *Geophys. Res. Lett.*, *29* (8),
859 doi:10.1029/2001GL014256, 1235.
860
861 Hutterli, M. A., J. R. McConnell, R. C. Bales, and R. W. Stewart (2003), Sensitivity of hydrogen
862 peroxide (H_2O_2) and formaldehyde (HCHO) preservation in snow to changing environmental
863 conditions: Implications for ice core records, *J. Geophys. Res.*, *108* (D1),
864 doi:10.1029/2002JD002528.
865
866 Isaksen, I. S. A., and O. Hov (1987), Calculation of trends in tropospheric O_3, OH CH_4, & NO_x,
867 *Tellus*, *39B*, 271-285.
868
869 Johnston, J. C., and M. H. Thiemens (1997), The isotopic composition of tropospheric ozone in
870 three environments, *J. Geophys. Res.*, *102* (D21), 25,395-25,404.

J. Jouzel, V. Masson-Delmotte, O. Cattani, G. Dreyfus, S. Falourd, G. Hoffmann, B. Minster, J. Nouet, J. M. Barnola, J. Chappellaz, H. Fischer, J. C. Gallet, S. Johnsen, M. Leuenberger, L. Loulergue, D. Luethi, H. Oerter, F. Parrenin, G. Raisbeck, D. Raynaud, A. Schilt, J. Schwander, E. Selmo, R. Souchez, R. Spahni, B. Stauffer, J. P. Steffensen, B. Stenni, T. F. Stocker, J. L. Tison, M. Werner, and E. W. Wolff (2007), Orbital and Millennial Antarctic Climate Variability over the Past 800,000 Years, *Science*, *317*, 793-796.

Kames, J., and U. Schurath (1995), Henry's Law and Hydrolysis-Rate Constants for Peroxyacyl Nitrates (PANs) Using a Homogeneous Gas-Phase Source, *J. Atmos. Chem.*, *21*, 151-164.

Kaplan, J. O. (2002), Wetlands at the Last Glacial Maximum: Distribution and methane emissions, *Geophys. Res. Lett.*, *29* (6), doi:10.1029/2001GL013366, 1079.

Kaplan, J. O., G. Folberth, and D. A. Hauglustaine (2006), Role of methane and biogenic volatile organic compound sources in late glacial and Holocene fluctuations of atmospheric methane concentrations, *Global Biogeochem. Cycles*, *20*, GB2016, doi:10.1029/2005GB002590.

Köhler, M. O., G. Rädel, O. Dessens, K. P. Shine, H. L. Rogers, O. Wild, and J. A. Pyle (2008), Impact of perturbations to nitrogen oxide emissions from global aviation, *J. Geophys. Res.*, *113*, D11305, doi:10.1029/2007JD009140.

Labrador, L. J., R. von Kuhlmann, and M. G. Lawrence (2004), Strong sensitivity of the global mean OH concentration and the tropospheric oxidizing efficiency to the source of NO_x from lightning, *Geophys. Res. Lett.*, *31*, L06102, doi:10.1029/2003GL019229.

897 Lathière, J., D. A Hauglustaine, and N. De Noblet-Ducoudré (2005), Past and future changes in
898 biogenic volatile organic compound emissions simulated with a global dynamic vegetation model,
899 *Geophys. Res. Lett.*, *32*, L20818, doi:10.1029/2005GL024164.
900
901 Law, K. S., and J. A. Pyle (1993), Modeling Trace Gas Budgets in the Troposphere. 1. Ozone and
902 Odd Nitrogen, *J. Geophys. Res.*, *98*, 18,377-18,400.
903
904 Lawrence, M. G., P. Jöckel, and R. von Kuhlmann (2001), What does the global mean OH
905 concentration tell us?, *Atmos. Chem. Phys.*, *1*, 37-49.
906
907 Lelieveld, J., T. M. Butler, J. N. Crowley, T. J. Dillon, H. Fischer, L. Ganzeveld, H. Harder, M. G.
908 Lawrence, M. Martinez, D. Taraborrelli, and J. Williams (2008), Atmospheric oxidation capacity
909 sustained by a tropical forest, Letters to Nature, *Nature*, *452*, doi:10.1038/nature06870, 737-740.
910
911 Levine, J. G., P. Braesicke, N. R. P. Harris, N. H. Savage, and J. A. Pyle (2007), Pathways and
912 timescales for troposphere-to-stratosphere transport via the tropical tropopause layer and their
913 relevance for very short lived substances, *J. Geophys. Res.*, *112*, doi:10.1029/2005JD006940.
914
915 Loulergue, L., A. Schilt, R. Spahni, V. Masson-Delmotte, T. Blunier, B. Lemieux, J.-M. Barnola,
916 D. Raynaud, T. F. Stocker, and J. Chappellaz (2008), Orbital and millennial-scale features of
917 atmospheric CH_4 over the past 800,000 years, Letters to Nature, *Nature*, *453*, 383-386.
918
919 Lyons, J. R. (2001), Mass-independent fractionation of oxygen-containing radicals in the
920 atmosphere, *Geophys. Res. Lett.*, *28* (17), 3231-3234.
921

922 MARGO Project Members (2009), Constraints on the magnitude and patterns of ocean cooling at
923 the last glacial maximum, *Nature Geoscience*, *2*, doi:10.1038/ngeo411, 127-132.
924
925 Martinerie, P., G. P. Brasseur, and C. Granier (1995), The chemical composition of ancient
926 atmospheres: A model study constrained by ice core data, *J. Geophys. Res.*, *100*, D7, 14,291-
927 14,304.
928
929 Monnin, E., A. Indermuhle, A. Dallenbach, J. Fluckiger, B. Stauffer, T. F. Stocker, D. Raynaud,
930 and J. M. Barnola (2001), Atmospheric CO2 concentrations over the last glacial termination,
931 *Science*, *291*, 112–114.
932
933 Otto-Bliesner, B. L., R. Schneider, E. C. Brady, M. Kucera, A. Abe-Ouchi, E. Bard, P. Braconnot,
934 M. Crucifix, C. D. Hewitt, M. Kageyama, O. Marti, A. Paul, A. Rosell-Melé, C. Waelbroeck, S. L.
935 Weber, M. Weinelt, and Y. Yu (2009), A comparison of PMIP2 model simulations and the
936 MARGO proxy reconstruction for tropical sea surface temperatures at last glacial maximum, *Clim.*
937 *Dyn.*, *32*, doi:10.1007/s00382-008-0509-0, 799-815.
938
939 Platt, U., W. Allan, and D. Lowe (2004), Hemispheric average Cl atom concentration from $^{13}C/^{12}C$
940 ratios in atmospheric methane, *Atmos. Chem. Phys.*, *4*, 2393-2399.
941
942 Pöschl, U., R. von Kuhlmann, N. Poisson, and P. J. Crutzen (2000), Development and
943 intercomparison of condensed isoprene oxidation mechanisms for global atmospheric modeling, *J.*
944 *Atmos. Chem.*, *37*, 29–52.
945
946 Power, M. J., J. Marlon, N. Ortiz, P. J. Bartlein, S. P. Harrison, F. E. Mayle, A. Ballouche, R. H. W.
947 Bradshaw, C. Carcaillet, C. Cordova, S. Mooney, P. I. Moreno, I. C. Prentice, K. Thonicke, W.

948 Tinner, C. Whitlock, Y. Zhang, Y. Zhao, A. A. Ali, R. S. Anderson, R. Beer, H. Behling, C. Briles,
949 K. J. Brown, A. Brunelle, M. Bush, P. Camill, G. Q. Chu, J. Clark, D. Colombaroli, S. Connor, A.-
950 L. Daniau, M. Daniels, J. Dodson, E. Doughty, M. E. Edwards, W. Finsinger, D. Foster, J.
951 Frechette, M.-J. Gaillard, D. G. Gavin, E. Gobet, S. Haberle, D. J. Hallett, P. Higuera, G. Hope, S.
952 Horn, J. Inoue, P. Kaltenrieder, L. Kennedy, Z. C. Kong, C. Larsen, C. J. Long, J. Lynch, E. A.
953 Lynch, M. McGlone, S. Meeks, S. Mensing, G. Meyer, T. Minckley, J. Mohr, D. M. Nelson, J.
954 New, R. Newnham, R. Noti, W. Oswald, J. Pierce, P. J. H. Richard, C. Rowe, M. F. Sanchez Goñi,
955 B. N. Shuman, H. Takahara, J. Toney, C. Turney, D. H. Urrego-Sanchez, C. Umbanhowar, M.
956 Vandergoes, B. Vanniere, E. Vescovi, M. Walsh, X. Wang, N. Williams, J. Wilmshurst, and J. H.
957 Zhang (2008), Changes in fire regimes since the Last Glacial Maximum: an assessment based on a
958 global synthesis and analysis of charcoal data, *Clim. Dyn.*, *30*, doi: 10.1007/s00382-007-0334-x.
959
960 Prather, M. J. (1986), Numerical advection by conservation of second-order moments, *J. Geophys.*
961 *Res.*, *91*, 6671-6681.
962
963 Prather, M. J. (1996), Time scales in atmospheric chemistry: Theory, GWPs for CH_4 and CO, and
964 runaway growth, *Geophys. Res. Lett.*, *23* (19), 2,597-2,600.
965
966 Röckmann, T., Brenninkmeijer, C. A. M., P. Neeb, and P. J. Crutzen (1998a), Ozonolysis of
967 nonmethane hydrocarbons as a source of the observed mass independent oxygen isotope
968 enrichment in tropospheric CO, J. Geophys. Res., 103, D1, 1463-1470.
969
970 Röckmann, T., C. A. M. Brenninkmeijer, G. Saueressig, P. Bergamaschi, J. N. Crowley, H. Fisher,
971 and P. J. Crutzen (1998b), Mass-independent oxygen isotope fractionation in atmospheric CO as a
972 result of the reaction CO + OH, *Science*, *281*, 544-546.
973

974 Savarino, J., and M. H. Thiemens (1999), Analytical procedure to determine both $\delta^{18}O$ and $\delta^{17}O$ of
975 H_2O_2 in natural water and first measurements, *Atmos. Environ.*, 33,3683-33,3690.
976
977 Savarino, J., C. C. W. Lee and M. H. Thiemens (2000), Laboratory oxygen isotopic study of
978 sulphur (IV) oxidation: Origin of the mass-independent oxygen isotopic anomaly in atmospheric
979 sulfates and sulphate mineral deposits on Earth, *J. Geophys. Res.*, *105*, 29,079-29,088.
980
981 Savarino, J., S. Bekki, J. Cole-Dai, and M. H. Thiemens (2003), Evidence from sulphate mass
982 independent oxygen isotopic compositions of dramatic changes in atmospheric oxidation following
983 massive volcanic eruptions, *J. Geophys. Res.*, *108* (D21), doi:10.1029/2003JD003737, 4671.
984
985 Seinfeld, J. H., and S. N. Pandis (1998), Chemistry of the atmospheric aqueous phase in
986 *Atmospheric Chemistry and Physics: From Air Pollution to Climate Change,* Wiley-Interscience,
987 New York.
988
989 Severinghaus, J. P., T. Sowers, E. J. Brook, R. B. Alley, and M. L. Bender (1998), Timing of abrupt
990 climate change at the end of the Younger Dryas interval from thermally fractionated gases in polar
991 ice, *Nature*, *391*, 141-146.
992
993 Staffelbach, T., A. Neftel, B. Stauffer, and D. Jacob (1991), A record of the atmospheric methane
994 sink from formaldehyde in polar ice cores, Letters to Nature, *Nature*, *349*, 603-605.
995
996 Stockwell, D. Z., C. Giannakopoulos, P.-H. Plantevin, G. D. Carver, M. P. Chipperfield, K. S.
997 Law, J. A. Pyle, D. E. Shallcross, and K. Y. Wang (1999), Modelling NOx from lightning and its
998 impact 5 on global chemical fields, *Atmos. Environ.*, *33*, 4477-4493.
999

1000 Sumner, A. L., and P. B. Shepson (1999), Snowpack production of formaldehyde and its effect on
1001 the Arctic troposphere, Letters to Nature, *Nature*, *398*, 230-233.
1002
1003 Thonicke, K., I. C. Prentice, and C. Hewitt (2005), Modeling glacial-interglacial changes in global
1004 fire regimes and trace gas emissions, *Global Biogeochem. Cycles*, *19*, GB3008,
1005 doi:10.1029/2004GB002278.
1006
1007 Tiedtke, M. (1989), A Comprehensive Mass Flux Scheme for Cumulus Parameterization in Large-
1008 Scale Models, *Mon. Weather Rev.*, *117*, 1779-1800.
1009
1010 Valdes, P. J., D. J. Beerling, and C. E. Johnson (2005), The ice age methane budget, *Geophys. Res.*
1011 *Lett.*, *32*, L02704, doi:10.1029/2004GL021004.
1012
1013 Valentin, K. M. (1990), Numerical Modelling of the climatological and anthropogenic influences on
1014 the chemical composition of the troposphere since the last glacial maximum, Ph.D. Thesis,
1015 University of Mainz, Germany.
1016
1017 Verma, S., O. Boucher, M. S. Reddy, H. C. Upadhyaya, P. Le Van, F. S. Binkowski, and O. P.
1018 Sharma (2007), Modeling and analysis of aerosol processes in an interactive chemistry general
1019 circulation model, *J. Geophys. Res.*, *112*, D03207, doi:10.1029/2005JD006077.
1020
1021 Walton, J. J., M. C. McCracken, and S. J. Ghan (1988), A global scale Lagrangian trace species
1022 model of transport, transformation and removal processes, *J. Geophys. Res.*, *93*, 8339-8354.
1023

1024 Wang, K. Y., J. A. Pyle, M. G. Sanderson, and C. Bridgeman (1999), Implementation of a
1025 convective atmospheric boundary layer scheme in a tropospheric chemistry transport model, *J.*
1026 *Geophys. Res.*, *104*, 23,729-23,745.
1027
1028 Warwick, N. J., S. Bekki, K. S. Law, E. G. Nisbet, and J. A. Pyle (2002), The impact of
1029 meteorology on the interannual growth rate of atmospheric methane, *Geophys. Res. Lett.*, *29*,
1030 doi:10.1029/2002GL015282.
1031
1032 Weber, S. L., A. J. Drury, W. H. J. Toonen, and M. van Weele (2010), Wetland methane emissions
1033 during the Last Glacial Maximum estimated from PMIP2 simulations: Climate, vegetation, and
1034 geographic controls, *J. Geophys. Res.*, *115*, D06111, doi:10.1029/2009JD012110.
1035
1036 Wild, O. (2007), Modelling the global tropospheric ozone budget: exploring the variability in
1037 current models, *Atmos. Chem. Phys.*, *7*, 2643–2660.
1038
1039 Wilkinson, M. J., R. K. Monson, N. Trahan, S. Lee, E. Brown, R. B. Jackson, H. W. Polleys, P. A.
1040 Fay, and R. Fall (2009), Leaf isoprene emission rate as a function of atmospheric CO_2
1041 concentration, *Glob. Change Biol.*, doi: 10.1111/j.1365-2486.2008.01803.x.
1042
1043 Yang, X., J. A. Pyle, and R. A. Cox (2008), Sea salt aerosol production and bromine release: Role
1044 of snow on sea ice, *Geophys. Res. Lett.*, *35*, L16815, doi:10.1029/2008GL034536.
1045
1046 Ziemke, J. R., and S. Chandra (2003), La Nina and El Nino-induced of ozone in the tropical lower
1047 atmosphere during 1970-2001, *Geophys. Res. Lett.*, *30* (3), 1142.
1048

Table 1. Trace gas emissions used in the PI model run, expressed in terms of molecular mass (Tg) per year. Except for the emissions of NO_2 from lightning, these emissions are as close as practically possible to those used by Valdes et al. [2005] in their study of the LGM-PI change in methane, using the STOCHEM chemistry-transport model; see Section 2.2 for more details.

Table 2. The annual-mean concentration (volume mixing ratio) of each chemical species in the AntBL calculated in the PI model run, and the percentage change in this concentration calculated in each sensitivity experiment; see Section 3.2 for more details. The species in parentheses are 'lumped species' from the Mainz isoprene mechanism [Pöschl et al., 2000].

Table 3. Modeled and estimated percentage changes in the concentration of OH in the AntBL, in each sensitivity experiment, relative to the PI model run. The estimated changes in OH are calculated based on the modeled changes in the annual-mean AntBL concentrations of HCHO and methane using the formula proposed by Staffelbach et al. [1991]; see Section 3.2 for more details.

Table 4. Percentage changes in the $[O_3]/[OH]$ and $[O_3]/[H_2O_2]$ ratios in the AntBL, $\Delta\,[O_3]/[OH]$ and $\Delta\,[O_3]/[H_2O_2]$ respectively, based on the changes in the annual-mean concentrations of OH, O_3 and H_2O_2 calculated in each sensitivity experiment, relative to the PI model run; see Section 3.2 for more details.

Figure 1. Distributions of the trace-gas emissions used in the PI model run, integrated over one year, expressed in terms of molecular mass (Tg) per grid box. They are as close as practically possible to those used by Valdes et al. [2005] in their study of the LGM-PI change in methane. NB The distribution of NO_2 emissions excludes those from lightning; see Section 2.2 for more details.

1074 **Figure 2.** Schematic illustration of the five sensitivity experiments, described in Section 2.3, each
1075 starting from the PI model setup, described in Section 2.2. In Source 1, the emissions of methane
1076 are reduced (ΔE_{CH4}) so as to reduce the annual-mean concentration of methane in the AntBL,
1077 [CH_4], to roughly that which characterized the LGM, whilst the rate of OH production is increased
1078 (ΔP_{OH}) in Sink 1 to effect the same change in [CH_4]. In Sink 2, all NMVOC emissions from
1079 vegetation are switched off (ΔE_{NMVOCs}), whilst the emissions of methane are reduced in Source 2
1080 ($\Delta E'_{CH4}$) to effect the same change in [CH_4]. Finally, in Sink+Source, all NMVOC emissions from
1081 vegetation are switched off (ΔE_{NMVOCs}) and the emissions of methane are reduced ($\Delta E''_{CH4}$) so as to
1082 reduce [CH_4] to roughly that which characterized the LGM, in line with Sink 1 and Source 1.
1083
1084 **Figure 3.** The monthly-mean concentration of methane modeled in the Arctic boundary layer
1085 (ArcBL) and the Antarctic boundary-layer (AntBL), plotted as a function of the meteorology used
1086 to drive the model in the PI run (top panel) and the five sensitivity experiments: Sink 1, Source 1
1087 and Sink+Source (bottom panel); Sink 2 and Source 2 (middle panel). In each case, the data shown
1088 correspond to the last three years of the run to 'chemical equilibrium' (3 x 1997) and the subsequent
1089 three-year run to gather data (1998-2000).
1090
1091 **Figure 4.** Measurements of methane concentration (blue line) and temperature (relative to the late
1092 Holocene; red line) from Dome C, Antarctica, spanning Dansgaard-Oeschger events 7 and 8
1093 (roughly 35 and 38ka before 1950); the data are taken from Loulergue et al. [2008] and Jouzel et al.
1094 [2007] respectively. The regions shaded grey indicate periods of 200 years at the beginning of
1095 these events, in which the concentration of methane changes by between 70 and 80 ppbv, or 15-
1096 20%, whilst the temperature, smoothed on a 200 year timescale (black line), hardly changes; see
1097 Section 4.5 for more details.
1098

Trace gas emissions used in the PI model run

Trace gas	Biomass burning	Oceans	Vegetation	Soil	Lightning	Wetlands	Termites	Total
NO_2	4.7	-	-	16.8	15.8	-	-	37.3
CH_4	11.0	13.0	-	-	-	147.9	27.0	198.9
CO	100.0	50.0	150.0	-	-	-	-	300.0
C_2H_6	0.7	-	3.5	-	-	-	-	4.2
C_3H_8	0.2	0.5	3.5	-	-	-	-	4.2
CH_3COCH_3	0.1	-	20.0	-	-	-	-	20.1
C_5H_8	-	-	673.7	-	-	-	-	673.7
C_2H_4	1.4	-	20.0	-	-	-	-	21.4
HCHO	0.3	-	-	-	-	-	-	0.3
CH_3CHO	0.8	-	-	-	-	-	-	0.8

Table 1. Trace gas emissions used in the PI model run, expressed in terms of molecular mass (Tg) per year. Except for the emissions of NO_2 from lightning, these emissions are as close as practically possible to those used by Valdes et al. [2005] in their study of the LGM-PI change in methane, using the STOCHEM chemistry-transport model; see Section 2.2 for more details.

Chemical composition of the PI AntBL and the changes calculated in each sensitivity experiment

Species (X)	$[X]_{PI}$ (vmr)	$\Delta[X]_{Sink1 - PI}$ (%)	$\Delta[X]_{Source1 - PI}$ (%)	$\Delta[X]_{Sink2 - PI}$ (%)	$\Delta[X]_{Source2 - PI}$ (%)	$\Delta[X]_{Sink+Source - PI}$
OH	5.27 (+/-0.61) E-15	+112 +/ 2	+19 +/- 1	+13 +/- 1	+7 +/- 0.3	+29 +/- 2
(ISON)	3.20 (+/-0.43) E-13	-74 +/ 1	-24 +/- 1	-100 +/- 0.0	-10 +/- 0.3	-100 +/- 0.0
HCOOH	1.78 (+/-0.46) E-13	-59 +/ 2	-10 +/- 0.3	-100 +/- 0.0	-4 +/- 0.1	-100 +/- 0.0
NALD	2.33 (+/-0.26) E-13	-64 +/ 1	-17 +/- 1	-100 +/- 0.0	-7 +/- 0.3	-100 +/- 0.0
(MACR)	5.71 (+/-1.56) E-14	-56 +/ 3	-12 +/- 0.3	-100 +/- 0.0	-5 +/- 0.1	-100 +/- 0.0
(ISOOH)	5.82 (+/-1.15) E-15	-67 +/ 6	-24 +/- 2	-100 +/- 0.0	-10 +/- 1	-100 +/- 0.0
MPAN	1.28 (+/-0.36) E-13	-60 +/ 2	-17 +/- 0.5	-100 +/- 0.0	-7 +/- 0.2	-100 +/- 0.0
C_5H_8	1.66 (+/-0.93) E-16	-51 +/ 11	-9 +/- 3	-100 +/- 0.0	-3 +/- 1	-100 +/- 0.0
HONO	2.26 (+/-0.21) E-15	+60 +/ 3	+17 +/- 0.4	-14 +/- 4	+6 +/- 0.2	-1 +/- 5
C_2H_6	1.21 (+/-0.05) E-10	-56 +/ 1	-15 +/- 1	-86 +/- 0.1	-6 +/- 0.2	-88 +/- 0.1
C_2H_4	7.14 (+/-0.54) E-12	-57 +/ 1	-16 +/- 0.4	-95 +/- 0.3	-7 +/- 0.1	-96 +/- 0.3
HACET	2.75 (+/-0.35) E-12	-50 +/ 3	-12 +/- 1	-100 +/- 0.0	-5 +/- 1	-100 +/- 0.0
C_3H_8	1.84 (+/-0.14) E-11	-49 +/ 1	-13 +/- 1	-52 +/- 0.3	-5 +/- 0.2	-57 +/- 0.5
CH_3CHO	6.25 (+/-0.12) E-13	-45 +/ 2	-9 +/- 1	-81 +/- 0.3	-4 +/- 0.3	-83 +/- 0.3
CH_3CO_3H	2.76 (+/-0.10) E-12	-39 +/ 2	-8 +/- 0.3	-94 +/- 0.1	-3 +/- 0.1	-94 +/- 0.1
PPAN	8.40 (+-/0.02) E-14	-34 +/ 3	-3 +/- 1	-76 +/- 2	-1 +/- 0.2	-77 +/- 1
CH_3OOH	7.94 (+/-0.73) E-11	-14 +/ 1	-44 +/- 0.3	-14 +/- 1	-18 +/- 0.2	-41 +/- 1
CO	3.35 (+/-0.10) E-08	-56 +/ 1	-26 +/- 1	-62 +/- 1	-11 +/- 0.3	-72 +/- 0.2
CH_3CH_2CHO	7.71 (+/-0.39) E-14	-37 +/ 2	-8 +/- 1	-55 +/- 1	-3 +/- 0.2	-57 +/- 0.3
PAN	1.34 (+/-0.07) E-11	-30 +/ 1	-1 +/- 0.1	-98 +/- 0.1	-0.3 +/- 0.1	-98 +/- 0.1
HCHO	1.28 (+/-0.11) E-11	-11 +/ 0.5	-40 +/- 0.1	-21 +/- 1	-16 +/- 0.0	-45 +/- 1
CH_3COCH_3	1.40 (+/-0.05) E-10	-32 +/ 2	-7 +/- 0.5	-93 +/- 0.1	-3 +/- 0.2	-93 +/- 0.1
H_2O_2	3.99 (+/-0.21) E-11	+8 +/ 0.4	-16 +/- 0.3	-38 +/- 1	-7 +/- 0.1	-46 +/- 1
CH_3CH_2OOH	5.63 (+/-0.15) E-13	-35 +/ 3	-11 +/- 0.2	-80 +/- 0.2	-4 +/- 0.1	-82 +/- 0.3
(MACROOH)	8.34 (+/-2.09) E-14	-41 +/ 3	-18 +/- 1	-100 +/- 0.0	-7 +/- 0.4	-100 +/- 0.0
CH_3CO_2H	2.01 (+/-0.11) E-12	-31 +/ 2	-9 +/- 0.2	-93 +/- 0.5	-3 +/- 0.1	-93 +/- 0.4
$CH_3(CH_2)_2OOH$	2.75 (+/-0.07) E-13	-32 +/ 2	-9 +/- 0.3	-43 +/- 0.4	-4 +/- 0.1	-46 +/- 1
$CH_3CH_2CH_2OOH$	9.64 (+/-0.19) E-14	-27 +/ 2	-8 +/- 0.3	-42 +/- 0.3	-3 +/- 0.1	-45 +/- 1
N_2O_5	1.55 (+/-0.21) E-14	-24 +/ 1	-7 +/- 1	-44 +/- 2	-3 +/- 1	-46 +/- 1
O_3	2.43 (+/-0.33) E-08	-19 +/ 2	-7 +/- 0.5	-22 +/- 3	-3 +/- 0.2	-27 +/- 4
HO_2NO_2	3.84 (+/-0.56) E-13	-24 +/ 2	-16 +/- 0.2	-35 +/- 3	-6 +/- 0.1	-44 +/- 3
CH_3ONO_2	3.53 (+/-0.06) E-12	-27 +/ 1	-33 +/- 0.3	-42 +/- 0.2	-13 +/- 0.1	-59 +/- 0.2
$HONO_2$	5.72 (+/-1.54) E-12	-5 +/ 2	-0.4 +/- 0.2	-13 +/- 5	-0.1 +/- 0.1	-14 +/- 5
CH_3COCH_2OOH	6.09 (+/-0.24) E-13	-0.4 +/ 4	-1 +/- 0.2	-91 +/- 0.2	-0.3 +/- 0.1	-91 +/- 0.2
CH_4	7.09 (+/-0.02) E-07	-52 +/ 0.1	-52 +/- 0.0	-22 +/- 0.1	-22 +/- 0.0	-52 +/- 0.1
MGLY	5.15 (+/-0.27) E-14	0.0 +/ 1	0.1 +/- 1	-97 +/- 0.4	-0.1 +/- 0.2	-97 +/- 0.4
H_2O	1.14 (+/-0.00) E-03	0.0 +/ 0.0	0.0 +/- 0.0	0.0 +/- 0.0	0.0 +/- 0.0	0 +/- 0.0

Table 2. The annual-mean concentration (volume mixing ratio) of each chemical species in the AntBL calculated in the PI model run, and the percentage change in this concentration calculated in

each sensitivity experiment; see Section 3.2 for more details. The species in parentheses are 'lumped species' from the Mainz isoprene mechanism [Pöschl et al., 2000].

Modeled and estimated changes in the concentration of OH in the AntBL

	$\Delta[OH]_{Sink1 - PI}$ (%)	$\Delta[OH]_{Source1 - PI}$ (%)	$\Delta[OH]_{Sink2 - PI}$ (%)	$\Delta[OH]_{Source2 - PI}$ (%)	$\Delta[OH]_{Sink+Source - PI}$ (%)
Modeled	+112	+19	+13	+7	+29
Estimated	+102	+27	+1	+9	+17

Table 3. Modeled and estimated percentage changes in the concentration of OH in the AntBL, in each sensitivity experiment, relative to the PI model run. The estimated changes in OH are calculated based on the modeled changes in the annual-mean AntBL concentrations of HCHO and methane using the formula proposed by Staffelbach et al. [1991]; see Section 3.2 for more details.

Modeled changes in the $[O_3]/[OH]$ and $[O_3]/[H_2O_2]$ ratios in the AntBL

	Sink 1	Source 1	Sink 2	Source 2	Sink+Source
Δ $[O_3]/[OH]$ (%)	-62	-22	-31	-9	-43
Δ $[O_3]/[H_2O_2]$ (%)	-25	+11	+26	+4	+36

Table 4. Percentage changes in the $[O_3]/[OH]$ and $[O_3]/[H_2O_2]$ ratios in the AntBL, Δ $[O_3]/[OH]$ and Δ $[O_3]/[H_2O_2]$ respectively, based on the changes in the annual-mean concentrations of OH, O_3 and H_2O_2 calculated in each sensitivity experiment, relative to the PI model run; see Section 3.2 for more details.

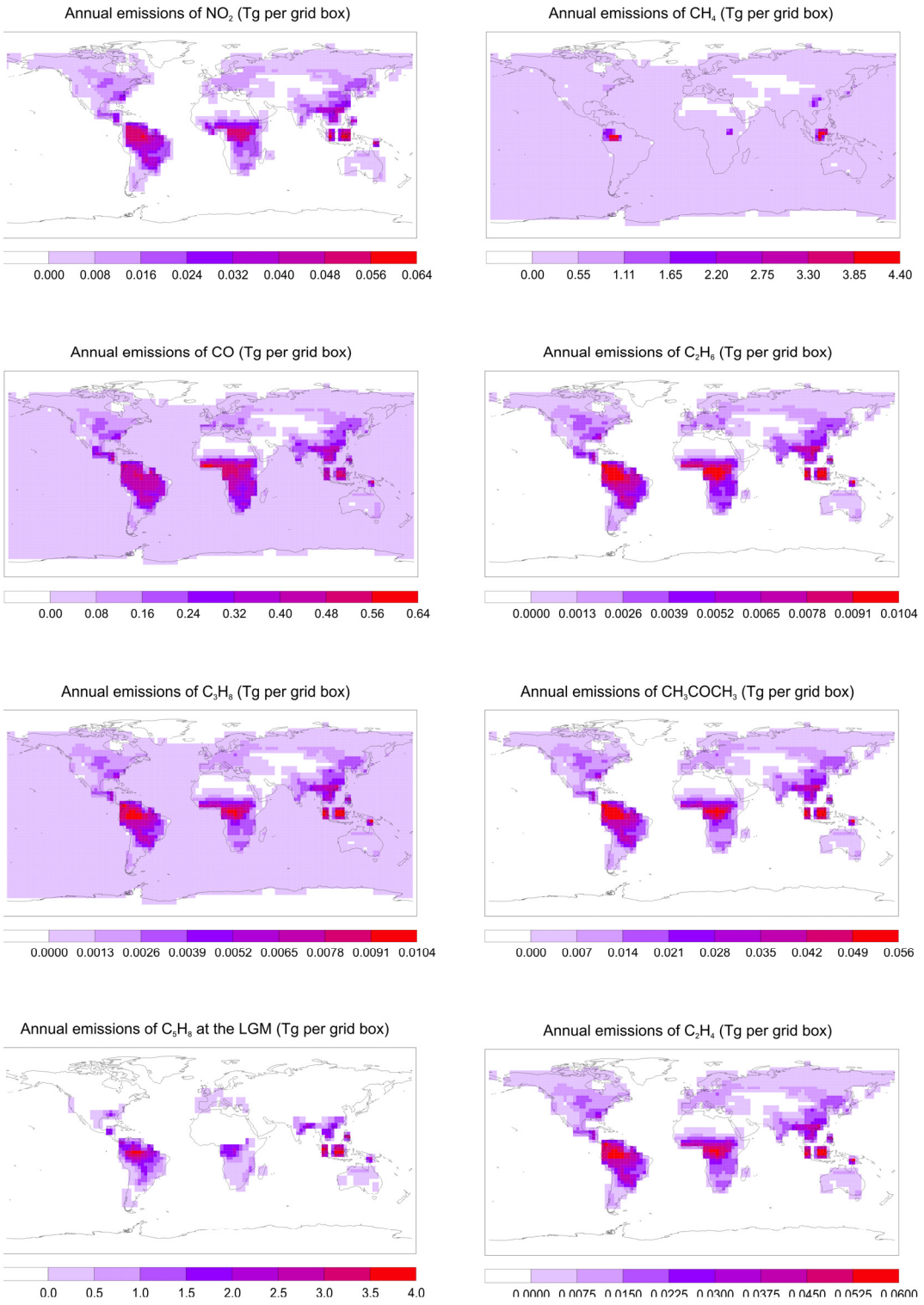

Figure 1. Distributions of the trace-gas emissions used in the PI model run, integrated over one year, expressed in terms of molecular mass (Tg) per grid box. They are as close as practically possible to those used by Valdes et al. [2005] in their study of the LGM-PI change in methane. NB The distribution of NO_2 emissions excludes those from lightning; see Section 2.2 for more details.

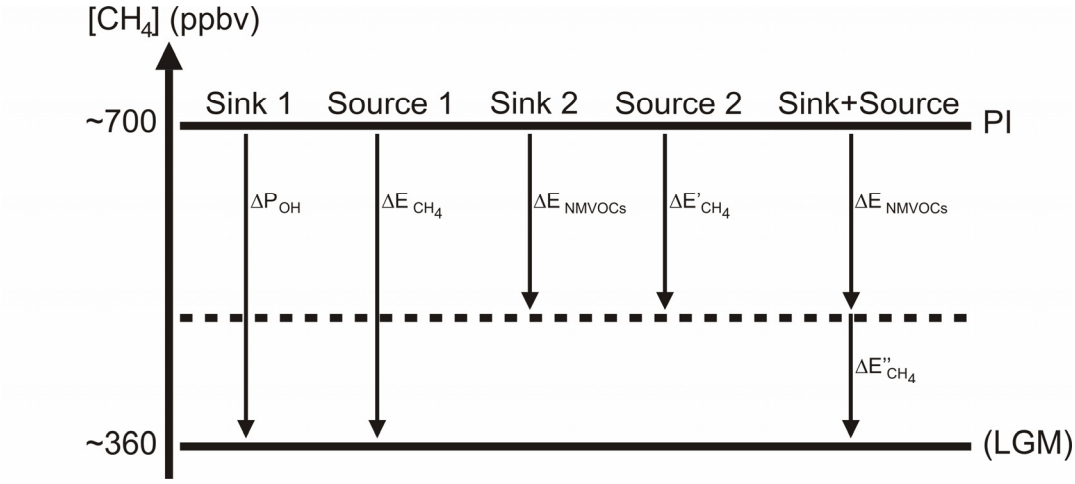

Figure 2. Schematic illustration of the five sensitivity experiments, described in Section 2.3, each starting from the PI model setup, described in Section 2.2. In Source 1, the emissions of methane are reduced (ΔE_{CH4}) so as to reduce the annual-mean concentration of methane in the AntBL, [CH_4], to roughly that which characterized the LGM, whilst the rate of OH production is increased (ΔP_{OH}) in Sink 1 to effect the same change in [CH_4]. In Sink 2, all NMVOC emissions from vegetation are switched off (ΔE_{NMVOCs}), whilst the emissions of methane are reduced in Source 2 ($\Delta E'_{CH4}$) to effect the same change in [CH_4]. Finally, in Sink+Source, all NMVOC emissions from vegetation are switched off (ΔE_{NMVOCs}) and the emissions of methane are reduced ($\Delta E''_{CH4}$) so as to reduce [CH_4] to roughly that which characterized the LGM, in line with Sink 1 and Source 1.

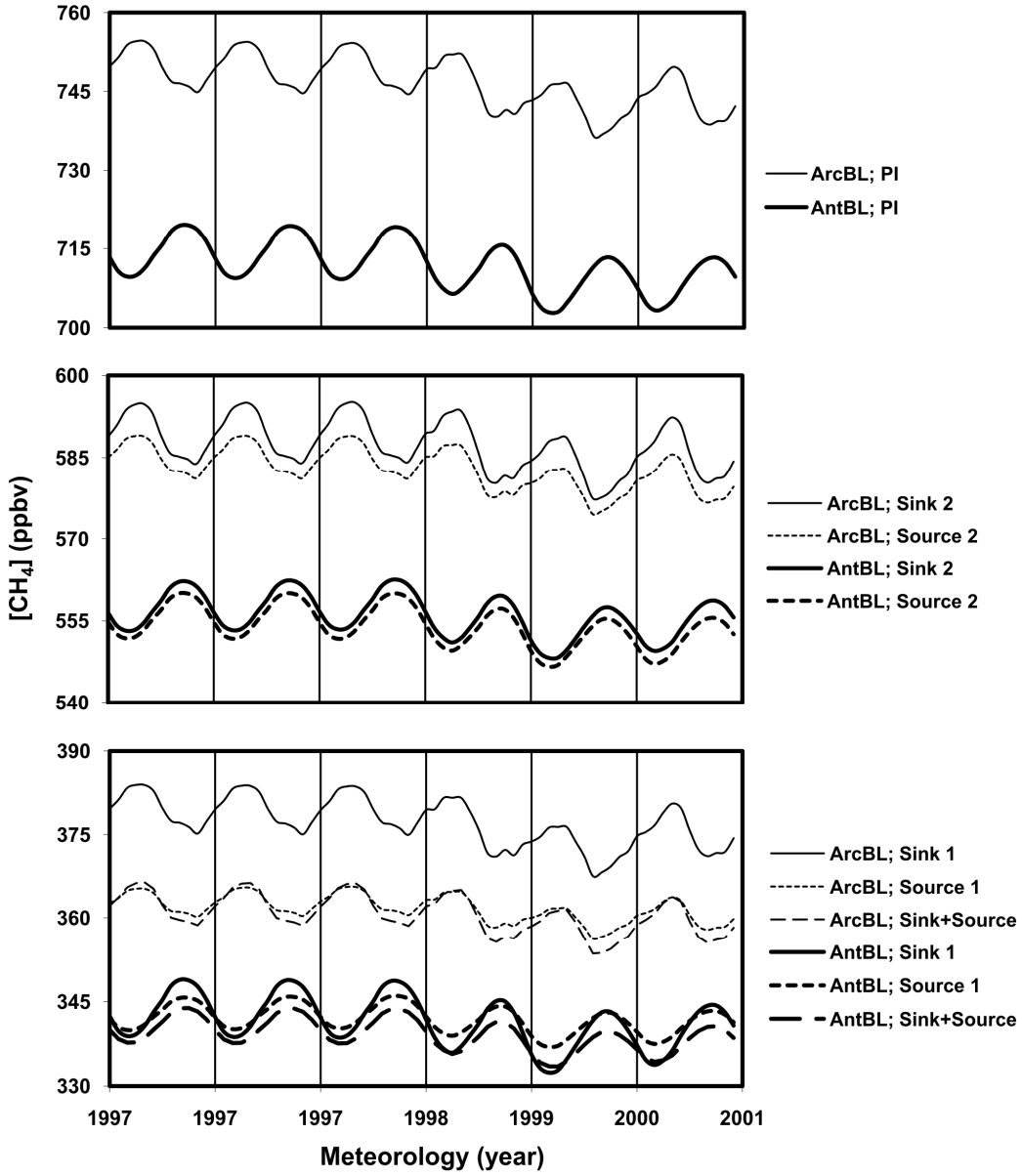

1149

1150

1151 **Figure 3.** The monthly-mean concentration of methane modeled in the Arctic boundary layer
1152 (ArcBL) and the Antarctic boundary-layer (AntBL), plotted as a function of the meteorology used
1153 to drive the model in the PI run (top panel) and the five sensitivity experiments: Sink 1, Source 1
1154 and Sink+Source (bottom panel); Sink 2 and Source 2 (middle panel). In each case, the data shown
1155 correspond to the last three years of the run to 'chemical equilibrium' (3 x 1997) and the subsequent
1156 three-year run to gather data (1998-2000).

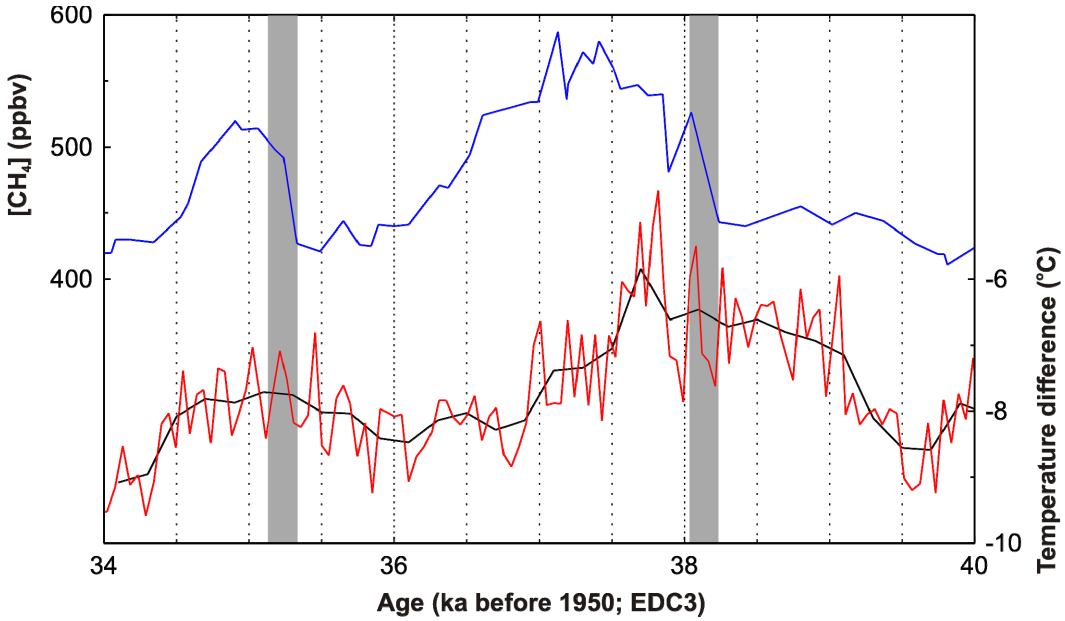

Figure 4. Measurements of methane concentration (blue line, top) and temperature (relative to the late Holocene; red line, bottom) from Dome C, Antarctica, spanning Dansgaard-Oeschger events 7 and 8 (roughly 35 and 38ka before 1950); the data are taken from Loulergue et al. [2008] and Jouzel et al. [2007] respectively. The regions shaded grey indicate periods of 200 years at the beginning of these events, in which the concentration of methane changes by between 70 and 80 ppbv, or 15-20%, whilst the temperature, smoothed on a 200 year timescale (black line), hardly changes; see Section 4.5 for more details.